We are IntechOpen, the world's leading publisher of Open Access books
Built by scientists, for scientists

4,500
Open access books available

118,000
International authors and editors

130M
Downloads

154
Countries delivered to

Our authors are among the

TOP 1%
most cited scientists

12.2%
Contributors from top 500 universities

CLARIVATE ANALYTICS
BOOK CITATION INDEX
INDEXED

WEB OF SCIENCE™

Selection of our books indexed in the Book Citation Index
in Web of Science™ Core Collection (BKCI)

Interested in publishing with us?
Contact book.department@intechopen.com

Numbers displayed above are based on latest data collected.
For more information visit www.intechopen.com

Passive Components for Ultra-Wide Band (UWB) Applications

Dalia N. Elsheakh and Esmat A. Abdallah

Abstract

UWB technology brings the convenience and mobility of wireless communications to very high-speed interconnects in the home and office due to the precision capabilities combined with the low power. This makes it ideal for certain radio frequency sensitive environments such as hospitals and healthcare as well as radars. UWB intrusion-detection radar is used for detecting through the wall and also used for security with fuse avoidance radar, precision locating and tracking (using distance measurements between radios), and precision time-of-arrival-based localization approaches. The FCC issued a ruling in 2002 that allowed intentional UWB emissions in the frequency range between 3.1 and 10.6 GHz, subject to certain restrictions for the emission power spectrum. Other definitions for ultra-wideband range of frequency are also used such as any device that has 500 MHz bandwidth or fractional bandwidth greater than 25% is considered an UWB enable high data rate to be transferred with a very low power that does not exceed -41.3 dBm.

The main advantage of UWB technology is that it has the ability to transmit high bandwidth data between various devices with distances in the order of 10 m far from each other, such as home or office appliances with high sped transfer which may reach 1Gbit/s.

There are many components that are designed and used in UWB systems such as antennas, power dividers/combiners, filters (LPF, BPF, etc.), rectennas, filtennas, etc.

Many types of antennas are able to achieve UWB. Monopole antennas are usually used as linearly polarized antennas which prove to be the best whelming choice for use in various automobiles and mobile equipment. Log parodic and Yagi antennas are other types of UWB with high gain. Electromagnetic band gap (EBG) structure as defected ground or split ring resonator are also used to improve the antenna bandwidth and achieve UWB.

Many UWB filters are designed and implemented using modern techniques such as meta-material, tuning stubs, defected ground structures, modified CMRC (compact microstrip resonant cell), etc. These filters may be switchable or tunable in order to make notch frequencies within the passband to provide interference immunity from unwanted radio signals, such as wireless local area networks (WLAN) and worldwide interoperability for microwave access (WiMAX) that cohabit within the UWB spectrum.

The need of compact multiband filtenna (filter combined with antenna) with the ability of covering the current standards at the microwave band and the next generation standards at the millimeter wave band simultaneously is raising. Also, the operation of cognitive radio and self-adaptive systems need to dynamically monitor the frequency spectrum in search of the unused licensed channels. All these applications need different types of filtenna which may be fixed, switchable or tunable that can operate in the

UWB range of frequency and also with narrow band modes to cover for example UWB/WiMAX applications.

Keywords: ultra-wide band (UWB), monopole antenna, UWB filters, filtenna, electromagnetic bandgap structure (EBG), log parodic

1. Introduction

In recent years, UWB technology has mostly focused on consumer electronics and wireless communications. Federal Communication Commission (FCC) issued a report in February 2002, allowing the commercial and unlicensed deployment of UWB applications in USA for both indoor and outdoor spectral mask. This wide frequency allocation initiated a lot of researches from both industry and academia [1]. UWB is used for short and medium range of radio communications and positioning applications.

The European regulatory body issue similar restrictions are shown in **Figure 1**. The key limitations for wireless communication using UWB are mentioned in [2–4].

UWB impulse radio system has several advantages over other conventional systems [5].

 i. High data rate wireless transmission: UWB systems can support more than 500 Mb/s data transmission rate in the range of 10 m, which enables for new services and applications.

 ii. High precision ranging: UWB systems have good time-domain resolution and it could be provided centimeter accuracy for location and tracking applications.

iii. UWB is used for location and tracking applications with cm accuracy.

 iv. UWB can operate under LOS and NLOS environments for signal penetrating obstacles.

 v. UWB system is capable of resistance to multipath fading.

 vi. The power spectral density is very low so it is secure and can coexist with other services such as WLAN, GPS, cellular system, etc.

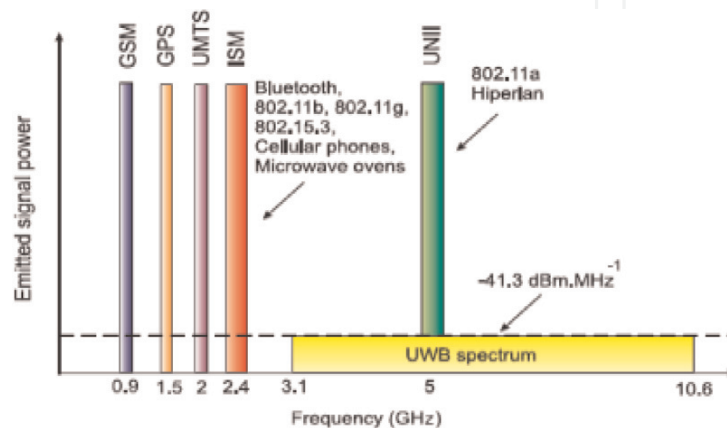vii. The UWB system has low cost due to using CMOS technology.

Figure 1.
European regulatory body spectrum.

Due to UWB technology and using nanosecond pulses in many applications such as military and biotechnology applications [6–8], the need for very broadband circularly polarized antenna has emerged. These UWB CP antennas are the substitution of the narrowband CP microstrip patch antennas [8–10].

One of the most commonly used devices to control the spectrum of radio frequency signals and necessary in an UWB radio system whether in impulse system or multiband system, in order to reconfigure the UWB signal to satisfy the spectrum regulation is the filter. Ultra-wide band (UWB) band-pass filter that achieves ultra bandwidth from 3.1 to 10.6, low insertion loss, low and flat group delay, out-band performance can be considered a well-designed UWB band-pass filter.

In UWB band-pass filters, one can use many techniques in their design such as composite low-pass and high-pass structure [11], multiple-mode resonator struc-ture [14], and short-circuited stub [12, 13]. Because UBW components occupy a large bandwidth which may be extended from 3.1 up to 10.6 GHz, interference attenuation due to coexisting services should be avoided. This is the motivation of using switchable or tunable narrow band notch within the passband of the UWB filter [15–17]. This may be achieved by many methods such as using additional notch resonators [18], embedded open stubs [19], asymmetric coupled fed lines [20], out-of-phase transmission cancelation [21], meander-line slots [22], and short-circuited stub resonators in a multilayer periodical structure [23].

To deal with different co-existed communication needs, the reconfigurable notch band implementation is required, but little research is concentrated on a UWB BPF with reconfigurable, switchable, or tunable notch bands as in [24–26].

An HFSS, FEM-based, 3D full wave electromagnetic solver simulator by ANSYS as well as CST were used for the design of all designed antennas. Also, ADS was used to design the filters and filtennas in addition to the above electromagnetic simulators in this chapter.

This chapter describes one example for printed millimeter wave antenna implementations, illustrating specific and interesting particular solutions for their design and two shapes of single UWB antenna in radio frequency range. In addition, two examples of UWB filters and one example of UWB filtennas are introduced.

2. UWB millimeter wave antenna

Classical antenna as reflector, lens, and horn type antennas have been used in millimeter-wave devices. But for low-cost, these antennas are commercial expensive devices, bulky, heavy and require complex feeding in an array system. In addition, they are very difficult to integrate with solid-state devices [6–9]. However, the microstrip antennas (MPAs) are narrow bandwidth and are large size about half-wavelength structures.

2.1 UWB slot antennas for linear and circular polarizations

Three different types of broad multi-band linearly and circularly polarized slot antennas (rectangular-, circular-, and triangular-shaped slots) for millimeter wave wireless communication applications [27] are shown in **Figures 2** and **3**, respec-tively. Proposed antenna consists of a slot radiator on the top metal layer and coupled to a rectangular dielectric resonator above the slot. The conventional microstrip-line-feed is used for different shapes of slot antennas. Final designed antennas were fabricated, and their characteristics were measured as reflection coefficient. The bandwidth of $|S_{11}| < -10$ dB was extended from 19.5 up to 75 GHz. This band covers wireless MM-wave applications and wireless networks, and the

WLAN, WPAN, and W-bands and most of 5th Generation mobile [28–32]. The average radiation efficiency and gain over the entire operating band are about 60% and 6 dBi, respectively [27]. Printed different shapes of slot antenna show small dimensions ($L_g \times W_g$) cut at different shapes of slots on larger conductor and are centered above the microstrip-feed line. The microstrip feed line is composed of a straight section of length L_f. To improve the antenna reflection coefficient response, a square stub slot is added with the side length $S = 0.6$ mm for further improvement in the antenna impedance matching as shown in **Figure 2**. The width of the tuning line is equal to that of the 50 Ω microstrip line ($W_f = 0.56$ mm). The optimized dimensions of the proposed antennas are shown in **Table 1**.

2.1.1 Linearly polarized antennas

The first shape of antenna design is either square with side length = 3.5 mm or rectangular slot with dimensions $L = 2.9$ mm and $W = 4$ mm as shown in **Figure 2 (a)**. The antenna reflection coefficient $|S_{11}|$ is shown in **Figure 4(a)**. **Figure 4(a)** shows that two antenna designs were examined with the same start and end of the operating resonate frequency band from 19.5 to 75 GHz. The square slot shaped antenna has bandwidth discontinuities from 34 to 45 GHz. The second shape included in this study is the circular and elliptical shaped slot as shown in
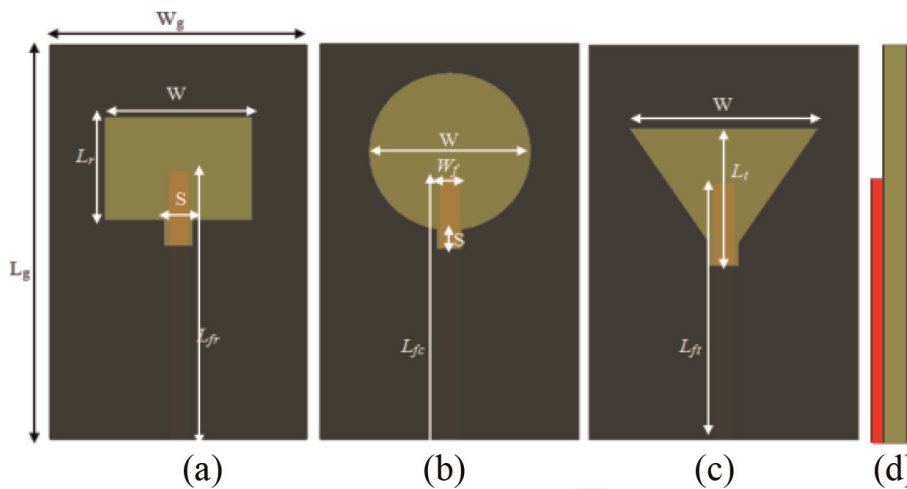

Figure 2.
Different shapes of slot antenna for LP (a) rectangular, (b) circular, (c) triangular, and (d) side view [27].
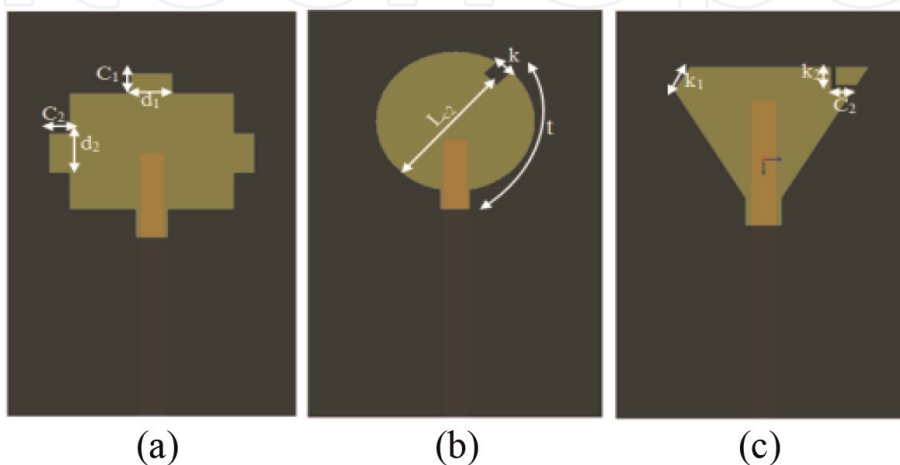

Figure 3.
Shapes of slot antenna for circular polarization (a) rectangular, (b) circular, and (c) triangular [27].

W_g	L_g	W	L_r	L_{ftc}	K	L_t	K_2	d_1	t
7	10	4	2.9	11.6	0.25	4.5	0.6	0.7	4.5
L_{fr}	L_{fc}	W_f	S	L_t	C_1	C_2	K_2	d_1	t
8.6	8.5	0.56	0.6	4	0.7	0.7	0.6	0.7	4.5

Table 1.
The optimized antennas (all dimensions in mm) [27].

Figure 2(b). The ellipse slot major diameter is W = 4 mm, and different radius ratios were used including the design with a ratio equal to 1.35 as shown in **Figure 4(b)**. The $|S_{11}|$ response shows that the optimal bandwidth at $|S_{11}| < -10$ dB is obtained using a circular slot shape. The bandwidth extends from 21 to 80 GHz in this case, while for the case of the elliptical slot, the bandwidth starts from 28 GHz and has the same end at 80 GHz as shown in **Figure 4(b)**. The triangular shape is the third slot shape used in this study, and it is compared to trapezoidal as an intermediate stage between a triangle and a rectangle slot as shown in **Figure 2(c)**. **Figure 4(c)** shows that both of the stated shapes resonate at frequencies higher than the other previous shapes, as it starts from 29 GHz.

2.1.2 Slot antennas for circularly polarized

Single-feed MPAs for CP are usually achieved by using traditional simple changes in the shape of the patch such as truncating corners, using nearly square or nearly circular patches, cutting a diagonal slot in the square or circular patches, protruding or inserting a pair of symmetric perturbation elements at the boundary of a circular patch [33–35]. However, this type produced narrow axial ratio (AR) bandwidth. The dual-fed and sequential array structure produced wider AR bandwidth, but this requires more complicated design and may occupy larger space. Slot antennas are expected to overcome the limited bandwidth problem as well as similar changes in the slot shape could be used to achieve CP.

Rectangular notches etched in the rectangular slot are used as a way to improve the 3 dB AR bandwidth as shown in **Figure 5(a)**. The notch width $C_1 = C_2 = 0.7$ mm gives the best wideband AR. The comparison of AR between measured and simulated is also shown in **Figure 5(a)**.

In the proposed design, a square stub with dimension side K was added to the circular shaped slot to achieve the CP performance. The stub is added at a radial distance t from square stub. The locations of this stub set the AR bandwidth without degrading the antenna performance as shown in **Figure 5(b)**. This figure shows that the stub with notch at a distance t = 3 mm gives the best performance AR
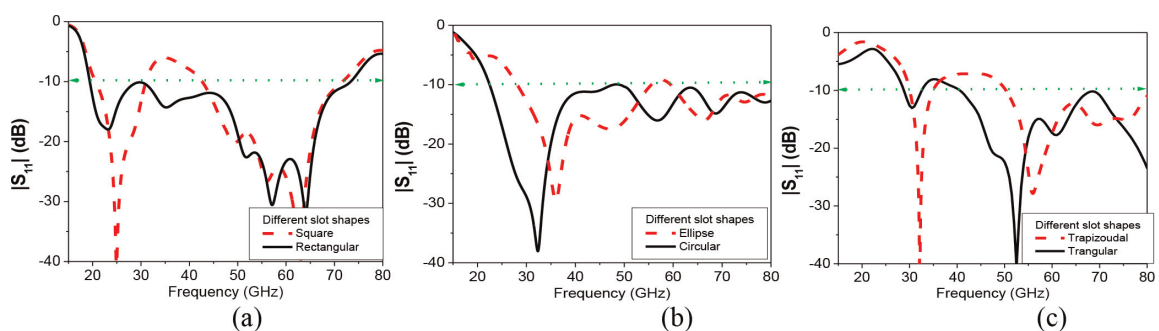

Figure 4.
Antenna $|S_{11}|$ response with different slot shapes (a) rectangular, (b) circular, and (c) triangular [27].
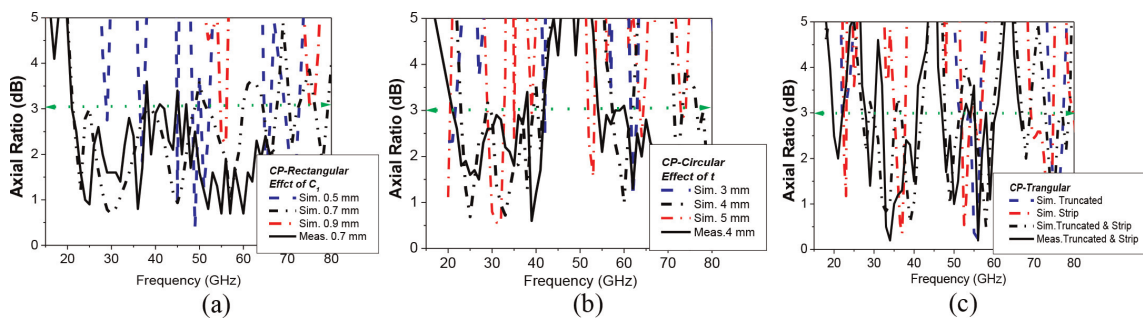
Figure 5.
Axial ratio of the antennas with different slot shapes (a) rectangular, (b) circular, and (c) triangular [27].

bandwidth. However, AR bandwidth discontinuities appear from 40 to 55 GHz. The comparison results of AR values simulated and measured at t = 3 mm is shown in **Figure 5(b)**. Finally, for the triangular slot shape, a truncated corner was used. To improve the AR bandwidth, an L-shaped strip was added at the other triangular corner with width 0.1 mm as shown in **Figure 3**. The bandwidth for simulated and measured AR values for the triangular CP antenna is shown in **Figure 5(c)**. From previous shapes, it appears that rectangular shaped slot with notches gives wide axial ratio bandwidth without degrading the antenna bandwidth.

2.1.3 Experimental results and discussion

The proposed antenna designs were fabricated by using milling machine technology with 0.1 mm accuracy on Rogers 6035HTC substrate with a 0.25 dielectric thickness and 0.017-mm copper thickness. A 1.85-mm end launcher connector is used to measure the proposed antennas. The simulation reflection coefficient was verified by comparison with the experimental results of the antennas by using 37397C Anritsu vector network analyzer. Photos of the fabricated antennas are shown in **Figures 6** and 7. The comparison between measured and simulated $|S_{11}|$ for linearly and circularly proposed antennas are shown in **Figure 8(i)** and **(ii)**, respectively. The measurement and simulation result data are in a good agreement. Measured results ended at 65 GHz as it is the end-point of the network analyzer. The rectangular slot shape gives the best antenna performance for linearly and circularly polarized slots. These designs also have low profile, wide impedance bandwidth $|S_{11}| < -10$ dB, and wide 3 dB axial ratio.
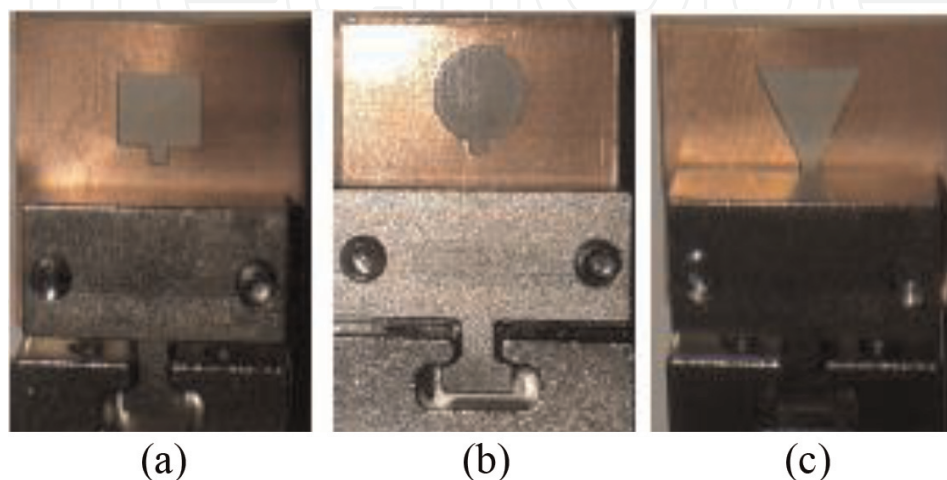

Figure 6.
Photo of fabricated linear polarized slot antenna, (a) rectangular, (b) circular, and (c) triangular shaped [27].
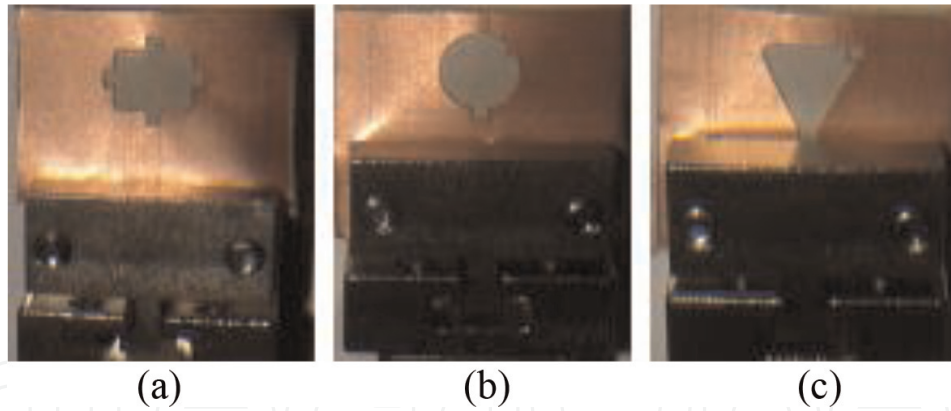
Figure 7.
Photo of fabricated circular polarized slot antenna, (a) rectangular, (b) circular, and
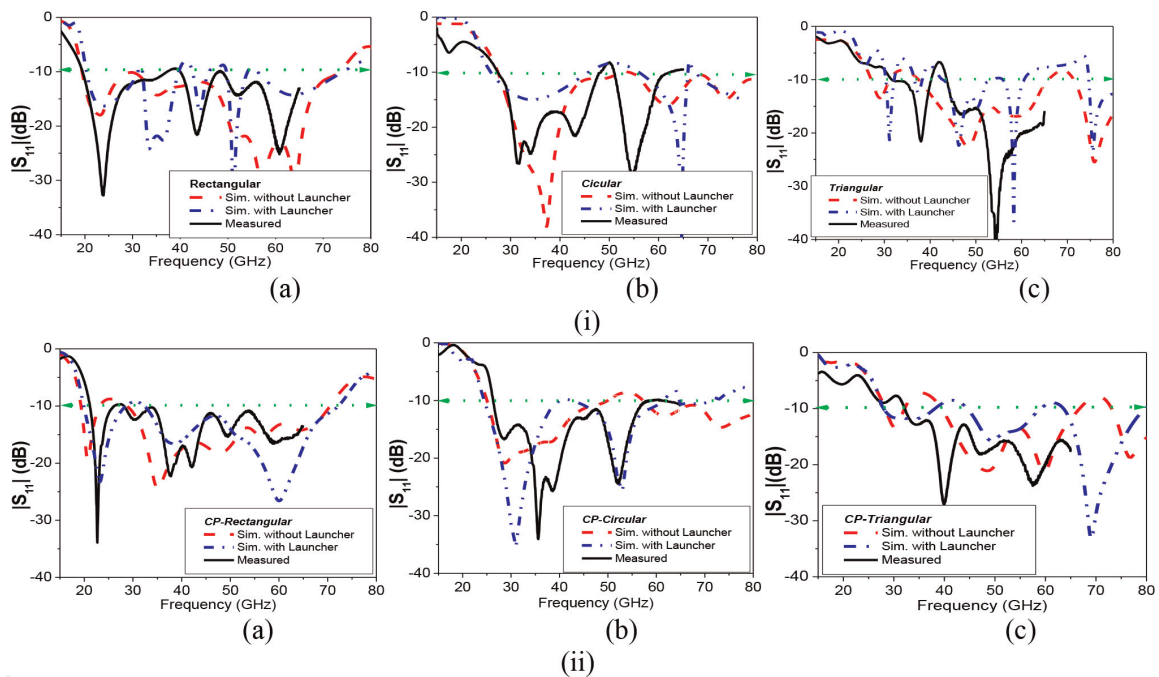*(c) triangular shaped [27].*

Figure 8.
Measured and simulated |S$_{11}$| of (i) linear polarized (a) rectangular, (b) circular, and (c) triangular slot
shaped and (ii) circular polarized (a) rectangular, (b) circular, and (c) triangular slot shaped [27].

3. UWB antenna in radio frequency range

Planar microwave circuitry has generated attractive radiating structures with high gain, low weight, reliability, ease of manufacturing and integration such as the Vivaldi antennas [36, 37], and the tapered slot antenna [38] for UWB antennas. The printed planar log-periodic dipole (LPDA) is the most suitable solution microwave frequencies [39]. LPDAs have a lot of advantages, such as directive radiation pattern, linear polarization and low cross polarization ratio over a wide frequency range [5]. At the beginning, coaxial cable was used for feeding the printed LPDAs at the radio and the TV frequency bands; however, it was found that the performance became worse when frequency increases. Due to huge increase in data traffic, there is a requirement for wireless networks which support both data and voice transfer simultaneously for short-range wireless communication systems [1, 2].

3.1 UWB CPW-fed LPDA for wireless applications

This section presents a LPDA for UWB applications [39]. The antenna consists of cascading four U-shaped elements of different line lengths with balun circuit to improve the antenna impedance matching. The proposed antenna area dimensions are 50×50 mm^2 built on FR4 substrate thickness 0.8 mm. Simulator HFSS is used for modeling the designed antenna. The pulse distortion is verified by measuring the proposed antenna performance with virtually steady group delay. The simulation and measurement results show that the designed antenna exhibits good impedance matching, stable radiation patterns throughout the whole operating frequency bands, acceptable gain and stable group delay over the entire operating band.

LPDA is UWB with the multiple resonance property; its bandwidth can be enhanced by increasing the number of the dipole elements [40–42]. Balanced structure, CPW fed antennas are very good candidates since the feed lines and the slots are on the same side of the substrate. There are many researches done to design LPDA but most of the published papers are not compact and their length is near from wavelength. The compact antenna dimensions, as shown in **Figure 9**, are $50 \times 50 \times 0.8$ mm^3. The proposed USLPDA antenna introduces USUWB with the multiple resonant property and compact size compared to earlier designs where UWB was realized using a rectangular slot [43], U-shaped dipole elements or stubs [38]. The bandwidth of this antenna at -10 dB reflection coefficient extends from 1.85 to 11 GHz which is wide enough to cover the FCC approved UWB in addition to wireless communications. The antenna exhibits good performance and can operate at wireless applications.

3.1.1 Geometry antenna and design

The designed geometry antenna is shown in **Figure 9**; the antenna is composed of four different lengths with U-shaped stubs. The lengths and spacing of the elements of LPDA increase logarithmically from one end to the other. The design of the LPDA is used where a wide range of frequencies is needed while still having moderate gain and directionality. The simulator HFSS is used to validate and optimize by simulating the designed antenna. The designed antenna is built on a commercial FR4 substrate with dielectric constant ε_r = 4.6, and loss tangent tan δ = 0.02. The antenna is fed by a 50 Ω transmission line, which can be easily integrated with other microwave circuits printed on the same substrate. For designing procedure,
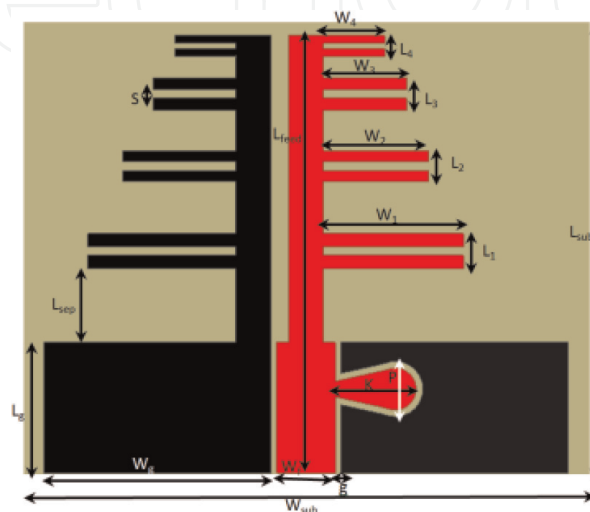

Figure 9.
Layout of the proposed log periodic dipole antenna (semi-LPDA) [39].

the number of trial steps is needed, the scale-factor τ, spacing factor δ, and the number of the dipole elements N should be determined. Second, the length of the longest arm, which responses to the lowest resonance frequency f_1, should be computed by following Eqs. (1)–(6) [39].

$$\frac{W_{i-1}}{W_i} = \tau \tag{1}$$

$$\delta = \frac{L_{isep}}{4W_i} \tag{2}$$

$$W_1 = \frac{\lambda_{1,eff}}{4} \tag{3}$$

$$N = 1 - (\ln B_s / \ln \tau) \tag{4}$$

$$B_a = 1.1 + 30.7\,\delta\,(1 - \tau) \tag{5}$$

$$B_s = B_a B_o \tag{6}$$

where λ_{1eff}, B_o, N, and int i are the longest effective operating wavelength, the operating frequency, number of elements, and i is an integer that varies from 2 to 5, respectively. To improve the impedance, matching the balun circuit with suitable dimensions is used as shown in **Figure 9**. **Table 2** introduces the dimensions of the proposed antenna [39].

3.1.2 Measured results

The designed antenna is fabricated by using photolithographic technique, as shown in **Figure 10**, and parameter performance is measured. The simulated and measured input reflection coefficient of the antennas is in good agreement, as shown in **Figure 10(b)**. The designed dipole impedance bandwidth at −10 dB of antenna extended from 1.85 to 11 GHz to cover most of the wireless applications and FCC UWB regulation. The antenna gain data are compared between measured and simulated results as shown in **Figure 11**. The designed LPDA antenna achieves simulated average gain 5.5 dBi, and the peak realized gain around 6.5 dBi at 2.7 GHz as shown in **Figure 11(a)**. The measured results show very good agreement with simulated results and about ±3 dBi difference on average over the operating band. Wheeler cap method [44] can be used to calculate the antenna radiation efficiency. The average radiation efficiency is around 70% over the operating band as shown in **Figure 11(b)**.

Then the radiation efficiency measured result is done by using horn antenna to complete the designed antenna radiation efficiency measurement as shown in **Figure 11(b)**. In the designed antenna, the radiator and the ground plane are contributing to radiation. For UWB applications, omnidirectional radiation pattern is an important requirement. At lower frequency band of operation, the pattern resembles a conventional dipole antenna, but at higher end of the UWB spectrum,

L_{sub}	L_g	W_{sub}	W_g	W_1	W_2	W_3	S	g	W_4
50	13.5	50	24	15.3	11.7	8.5	0.9	0.6	6
L_{sep}	L_4	L_{feed}	L_3	L_1	L_2	W_f	K	P	d
7.6	2.1	45	2.8	3.6	3	6	8.5	4.5	1000

Table 2.
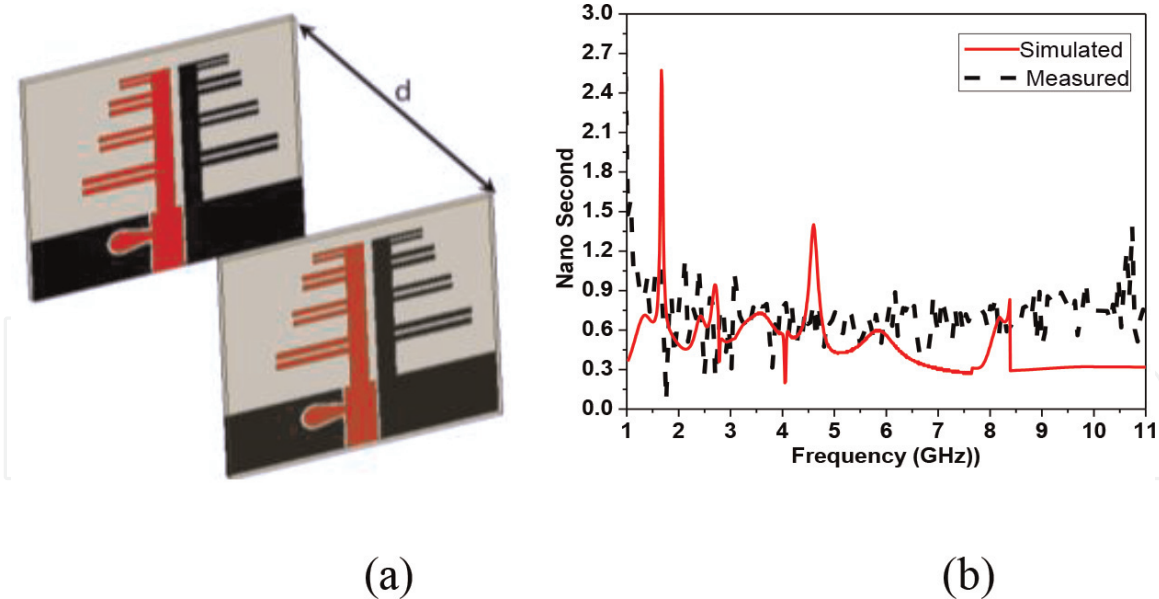*Dimensions of the proposed antenna (dimensions in mm) [39].*

Figure 10.
(a) GD simulated structures and (b) comparison between measured and simulated GD of LPDA [40].
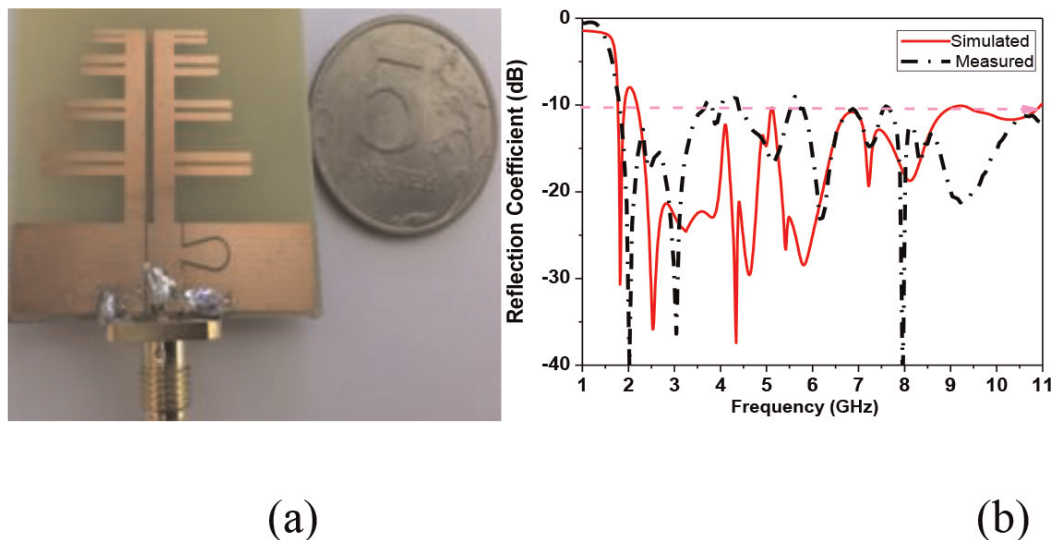

Figure 11.
(a) Fabricated LPDA antenna and (b) $|S_{11}|$comparison between simulated and measured results [40].

some ripples are observed which are attributed to higher order modes. There are discrepancies observed at higher frequency band spectrum, which arises due to measurement setup.

For UWB applications, group delay is an important factor in communication systems, for example, medical applications systems, security systems, and satellite communication systems, which are used for transmitting. To avoid occurring of distortion, it is recommended that the spectrum is treated in the same manner, over the proposed bandwidth of frequencies. When GD ripples are large, they may cause unsatisfactory distortion in the signal of a transmitting radio system. So, in radio system designs, there are specifications for how much a GD may be accepted. In nonlinear systems, nonlinear distortion happens since the magnitude of frequency response is not constant, and the phase response is nonlinear. The phase distortion could be used to measure GD, the phase characteristics must have a linear slope so that the ratio is constant for all frequencies and this represents a constant GD [44]. To measure the GD between two antennas with spacing d = 1 m, the usual practice
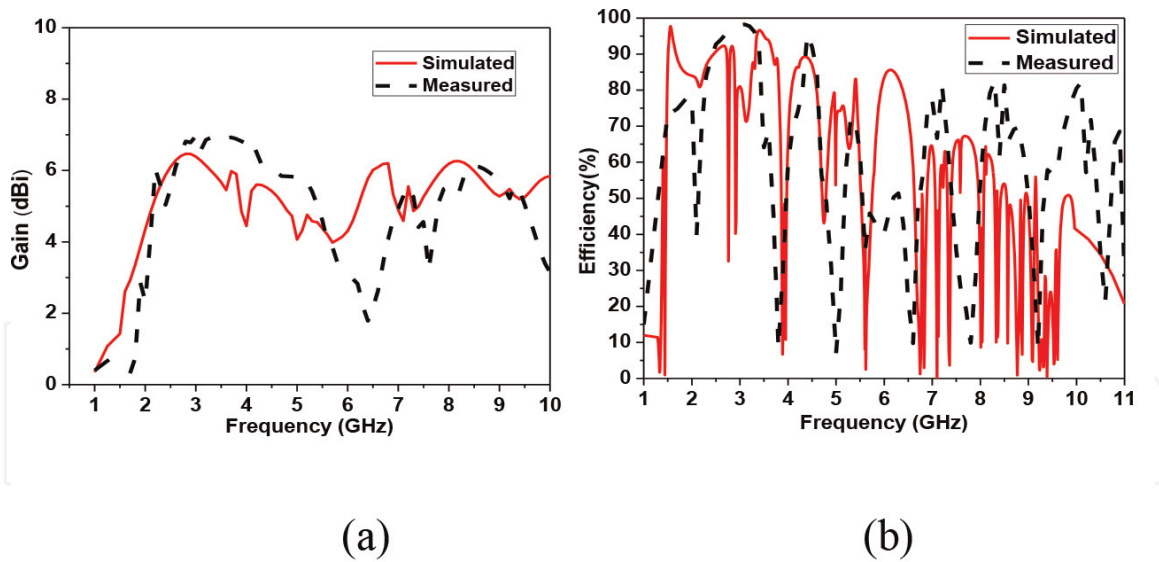
(a)   (b)

Figure 12.
Comparison between simulated and measured results (a) gain and (b) radiation efficiency of LPDA [40].

is to derive Q/ω for |S$_{21}$| phase. However, it is desirable that the same antenna is used for transition and receiving. High GD variations occur due to the steep phase shift over frequency, which may cause unsatisfactory distortions in the signal. **Figure 12** illustrates the simulated GD, and it can be noticed that the average group delay is about 1.5×10^{-9} second.

3.2 UWB monopole antenna using split ring resonator structure

This section presents designed steps to model an UWB monopole antenna. The designed antenna is composed of three different lengths of semi-circular shapes connected with circular disk and half circular modified ground plane. The designed antenna has an area equal 50 × 50 mm^2 on a low cost FR4 substrate [45]. The antenna demonstrates impedance bandwidth of −10 dB extended from 1.5 to 11 GHz with discontinuous bandwidth at different interior operating bands. Two pairs of SRR as metamaterial structure cells are inserted closely located from feeding transmission line of the antenna to achieve good impedance matching over the entire band of operation and improve the antenna performance. The fundamental parameters of the antenna including reflection coefficient, gain, radiation pattern, and group delay are obtained, and they meet the acceptable UWB antenna standard. Simulator HFSS ver. 14 is used as full wave electromagnetic solver then the prototypes are fabricated and measured. Results show that the antenna is very suitable for the applications in UWB as well as wireless communication systems.

For use in UWB systems, printed monopole patch antenna (PMPA) is an extremely attractive candidate because of its wide impedance bandwidth, omnidirectional azimuthal radiation pattern, low profile, and ease of integration with active devices and fabrication [46]. The design equation for lower band edge frequency has been reported in the literature. Moreover, these antennas are analyzed by using the frequency domain characteristics like return loss, gain, radiation pattern, surface current distribution, and group delay. Different narrowband services like WLAN, WiMax, GSM, UMTS, Wi-Fi, WMTS, ISM, UNII, DECT, European Hiper LAN I, II, and UWB (3.1–10.6 GHz) applications [1] could be obtained by using single UWB antenna.

A SRR is one of the electrically smallest resonant elements. It has many applications ranging from compact filters to advanced metamaterials. SRR has also a significant importance in electrically small antennas [46]. Metamaterials are good candidate for enhancement of the performances of different antennas. There are

varieties of SRR structures that have been reported in the literature like square, circular, triangular, omega, and labyrinth resonator [47].

3.2.1 Antenna structure and geometry

The designed antenna structure is composed of three connected semicircular arc monopoles with circular patch fed by microstrip transmission line and modified half circular shaped ground plane as shown in **Figure 13**. The initial design is validated and optimized by simulating the proposed antenna. The proposed antenna is designed on FR4 substrate with height 1.6 mm, dielectric constant ε_r = 4.6, and loss tangent tan δ = 0.02. The antenna is fed by a 50-Ω transmission line (TL).

3.2.2 Design and EM models with parametric study

The main design parameter for UWB antenna is the lower frequency edge (f_L) rather than the resonance frequency (f_r) as in Eq. (7). The lower band edge frequency of the designed antenna is calculated approximately by equating their surface area with that of an equivalent cylindrical monopole antenna of the same height as given by [45]. If R_1 is the height of the planar monopole antenna in cm, which is taken the same as that of an equivalent cylindrical monopole, and r in cm is the effective radius of the equivalent cylindrical monopole antenna, which is determined by equating area of the planar and cylindrical monopole antennas, then the lower band edge frequency is given as [45]:

$$f_L = \frac{7.2}{L_f + R_1 + r} GHz \tag{7}$$

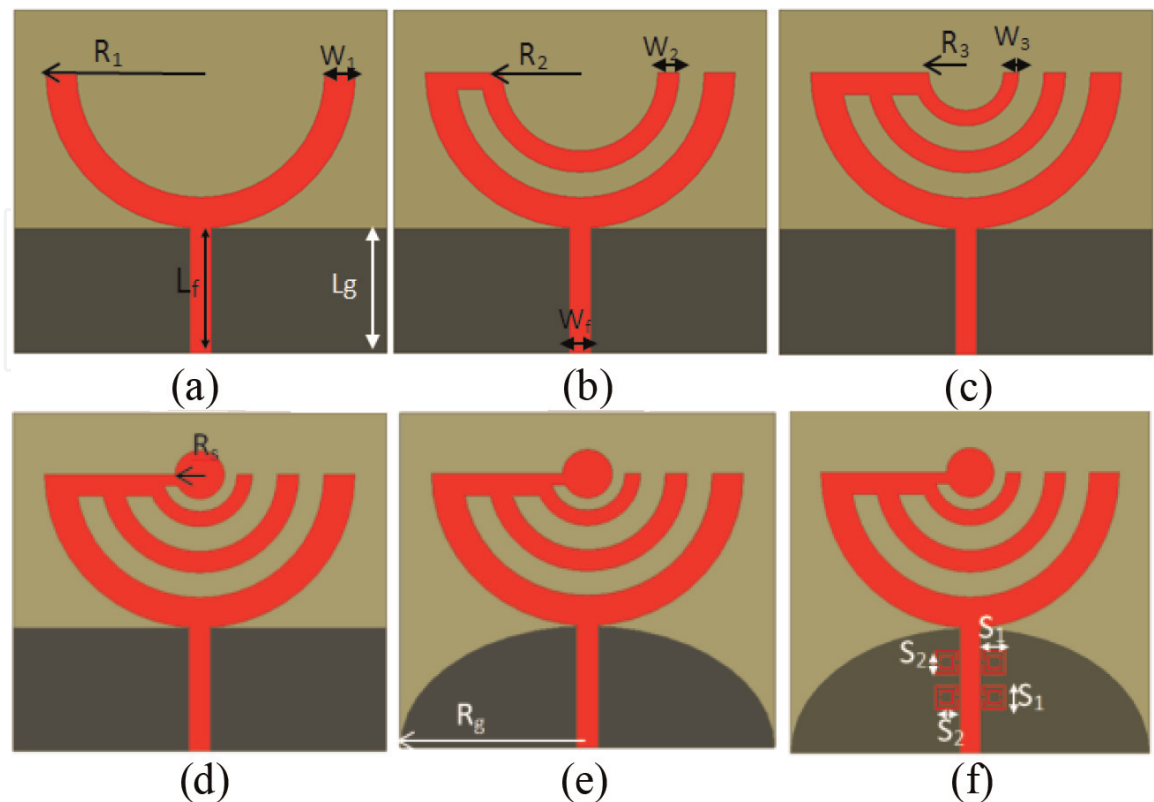where L_f is the length of the 50 Ω feed line in cm.

Figure 13.
Evolution of the design steps of the proposed printed monopole. (a) First step, (b) second step, (c) third step, (d) fourth step, (e) fifth step, and (f) sixth step [45].

The design started with first semi arc 180^0 with radius 25 mm and with 5 mm width modified ground plane L_g = 19 mm as shown in **Figure 13(a)**, and related $|S_{11}|$ is shown in **Figure 14**. To improve the bandwidth, second semi sector with radius 17 mm and width 3.5 mm as shown in **Figure 13(b)** with the same previous dimensions is added to add second resonant as shown in **Figure 14**. Third sector with radius 7.5 mm and width 2.5 mm is added, and keeping previous dimensions the same as shown in **Figure 13(c)**, a third resonance is achieved as shown in **Figure 14**. Another extension of the bandwidth is done by adding circular disk with radius 4 mm as shown in **Figure 13(d)**, and related reflection coefficient is shown in **Figure 14**. Modified ground plane is used to improve the bandwidth with ellipse with major radius 25 mm and minor radius 15 mm, as shown in **Figure 13(e)**, is suggested, and the related reflection is shown in **Figure 14**. The evolution of designing the proposed configuration is demonstrated in **Figure 13(f)**, and their corresponding optimized dimensions are tabulated in **Table 3**. The antenna gain and radiation efficiency are also studied as shown in **Figure 15**. The proposed antenna with SRR achieves an average gain of 7.5 dBi, and the peak realized gain around 22.5 dBi at 7.5 GHz as shown in **Figure 15(a)**. The designed antenna gain without SRR achieves an average gain around 5.5 dBi, while peak gain realized is 15 dBi at 8.5 and 10 GHz. The gain of the designed antenna is also measured, and there is good agreement between results especially at high frequency. The antenna radiation efficiency was simulated for both monopole antennas with and without SRR by using wheeler cap method [44]. The average radiation efficiency is around 70% over the operating bands for PMPA with SRR and around 65% without SRR as shown in **Figure 15(b)**.
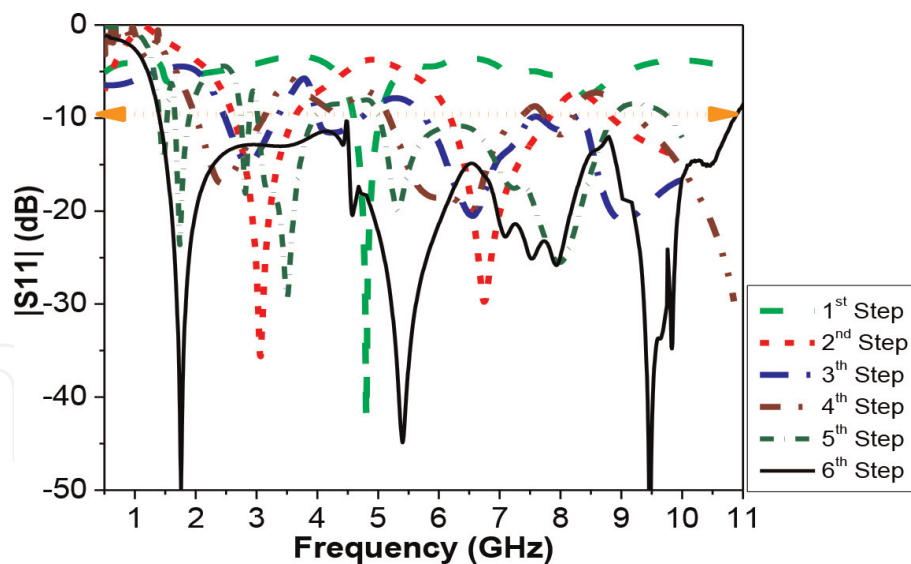

Figure 14.
Design procedures of the proposed antenna [45].

L_{sub}	W_{sub}	W_1	W_2	W_3	R_1	R_2
50	50	5	3.5	2.5	25	17
R_3	R_s	S_1	S_2	W_f	L_f	R_g
7.5	4	5	2.4	3	20	20

Table 3.
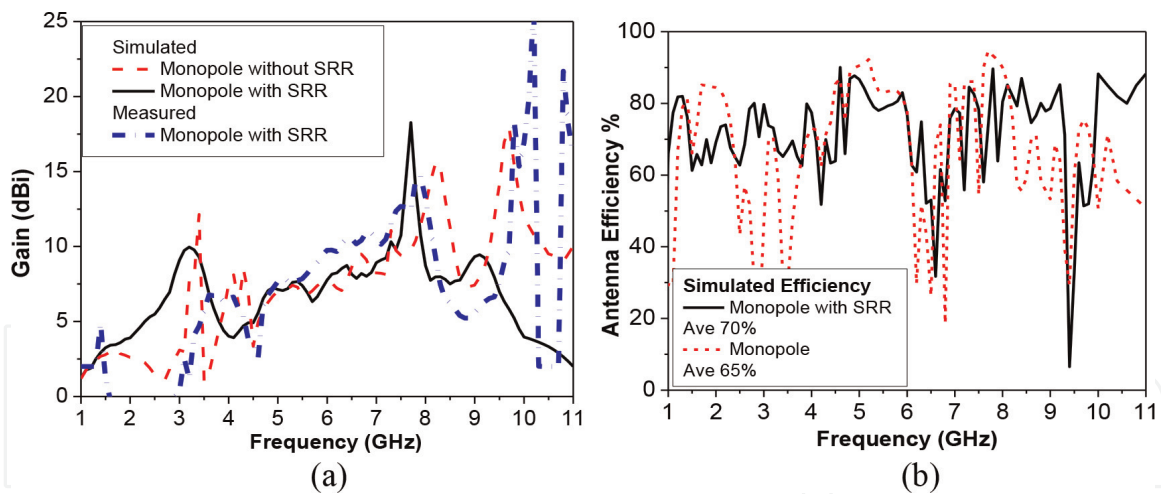*Dimensions of the proposed antenna (all dimensions in mm) [45].*

Figure 15.
(a) Antenna gain versus frequency and (b) simulated radiation efficiency with and without SRR [45].
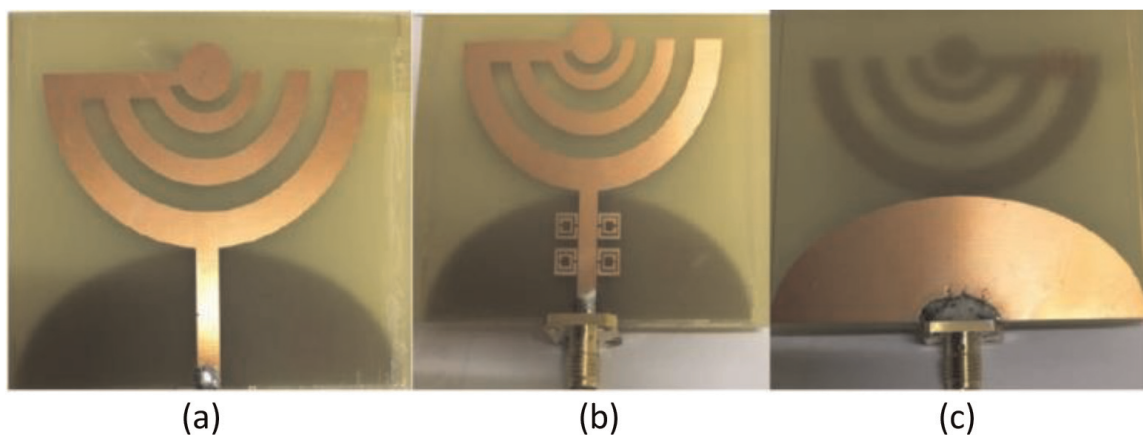

Figure 16.
Fabricated antenna (a) upper layer without SRR (b) upper layer with SRR, and (c) bottom layer [45].

3.2.3 Implementation and measured results

The prototype of the proposed antenna is shown in **Figure 16**. The performance parameters of the fabricated designed antennas are measured. The comparison results of simulated and measured input |S₁₁| of the antennas are found to be in very good agreement, as shown in **Figure 17**. The −10 dB bandwidth of the designed monopole antenna with SRR extended from 1.5 to 11 GHz to cover most wireless
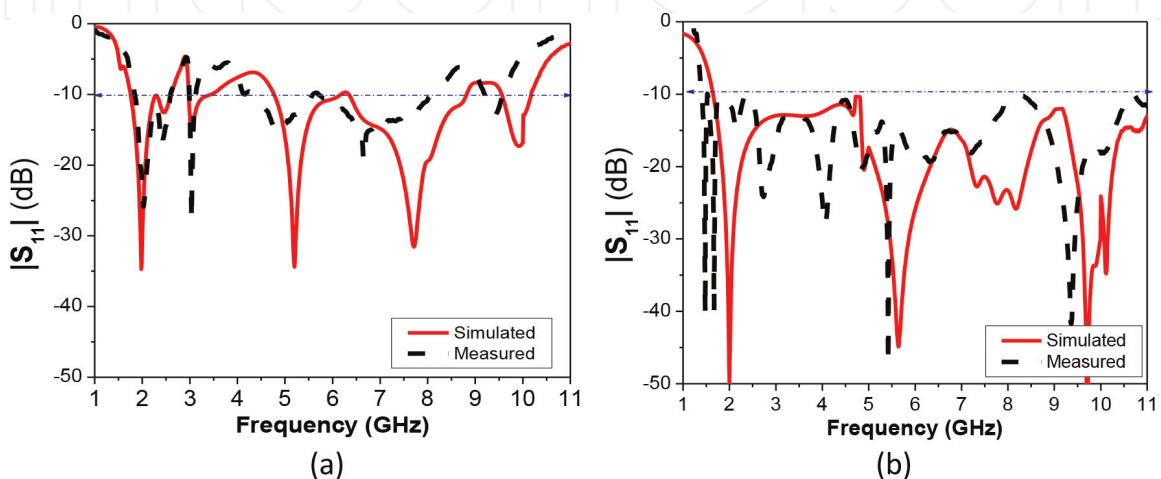

Figure 17.
Simulated and measured results of (a) monopole without SRR and (b) monopole with SRR [45].

application and FCC UWB regulation. It is fabricated by using photolithographic technique, and the measurements were carried out by using a Rohde & Schwarz ZVA67 vector network analyzer from 50 MHz to 67 GHz.

4. UWB filter

A filter is a two-port network that is used to control frequency response in a system. Filters can be classified into three main groups of active (requiring external power source), passive (no need for external power), and hybrid filters. Microwave systems are often involved with power conservation and noise control, and therefore, active filters are generally considered as last alternative. Passive filters are, however, further divided into lumped and distributed. The former consists of lumped components (including capacitors, inductors, resistors, and magnetic and electromechanical components), and the latter comprises a periodic conducting structure with various dielectric media. Inductors and capacitors form LC filters whereas resistors and capacitors form RC filters. Although resistors introduce loss to the circuit, they are generally used for broad banding (matching) purposes.

4.1 UWB band-pass filter with sharp tuned notched band rejection based on CRLH transmission-line unit cell

A compact UWB BPF with reconfigurable notch bands based on CRLH transmission line unit cell has been designed, simulated, and fabricated [48]. Two packages of software are used, namely, CST MWS and 3D EM commercial software HFSS version 13.0. The simulated and measured results are comparable. This filter has the advantage of very small size, and it also has four notched frequencies in its passband. The notched bands suppress the narrow-band services such as WLAN and WiMAX. One can control the center frequency of the notched band by varying the length L_6 of the stub. The total area of the filter is 16.4×5 mm^2. This small area makes it suitable for modern applications which need miniaturization.

4.1.1 Proposed filter design

The proposed filter is designed based on the filter described in Ref. [49] but with a new contribution which is notched controllable tunable four sharp rejection bands by adjusting the length of the coupling stub using diode switching matrix tools (instead of using PIN diodes).

Figure 18 shows the proposed microstrip UWB-BPF with tuned notched passband based on CRLH transmission-line unit cell. The optimized dimensions of the proposed filter are as shown in **Table 4**.

The dimension of the multi-mode section as shown in **Figure 18** is 4.4×1.5 mm, the length of the shunted inductive line is 3.1 mm, and the overall dimension of the proposed filter is 16.4×5.0 mm. Based on the above description, the design procedure can be as follows:

  i. The notched band depends on the coupling stub (L_6) in the output section.

 ii. The notch frequency of the filter can be changed by adjusting the length of the coupling stub L_6. As L_6 increases, the center notch frequency decreases as shown in **Table 5**. The length L_6 is controlled by using switching matrix equipment (mini circuit) where the character D refers to the diode.
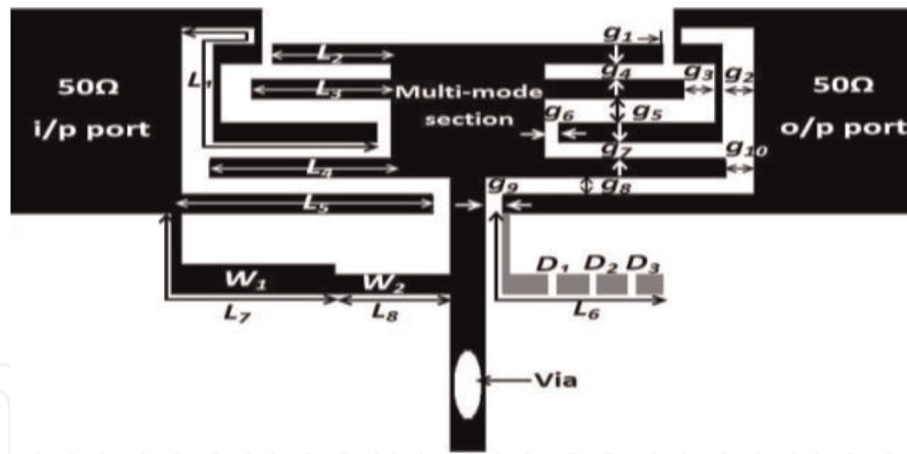
Figure 18.
The proposed filter [48].

L$_1$	L$_2$	L$_3$	L$_4$	L$_5$	L$_7$	L$_8$	w$_1$	w$_2$
9.3	3.4	4	5.2	7.2	5.3	3.3	0.3	0.2

g$_1$	g$_2$	g$_3$	g$_4$	g$_5$	g$_6$	g$_7$	g$_8$	g$_9$
0.3	0.9	0.9	0.2	0.3	0.4	0.2	0.2	0.5

Table 4.
Optimized dimensions of the proposed filter (all dimensions are in mm) [48].

Diode states	L$_6$ (mm)	f$_{notch}$ (GHz)
D1, D2, D3 (off)	2	6.18
D1(on), D2, D3 (off)	3.1	5.9
D1, D2(on), D3(off)	4.2	5.7
D1, D2, D3 (on)	5.3	5.5

Table 5.
(f$_{notch}$) against (L$_6$) variation [48].

4.1.2 Fabrication and measurements

The filter was fabricated using a photolithographic technique on Rogers RT/ Duroid 5880 with ε_r = 2.2, h = 0.787 mm, and tan δ = 0.0009. The photograph of the fabricated filter is shown in **Figure 19**. The measured and simulated S$_{11}$ and S$_{21}$ for different stub lengths are shown in **Figure 20(a)–(d)**. The UWB bandwidth extends between 3.1 and 10.6 GHz. There are four notched frequencies for the
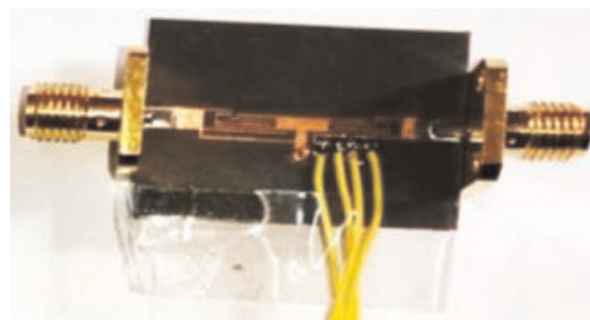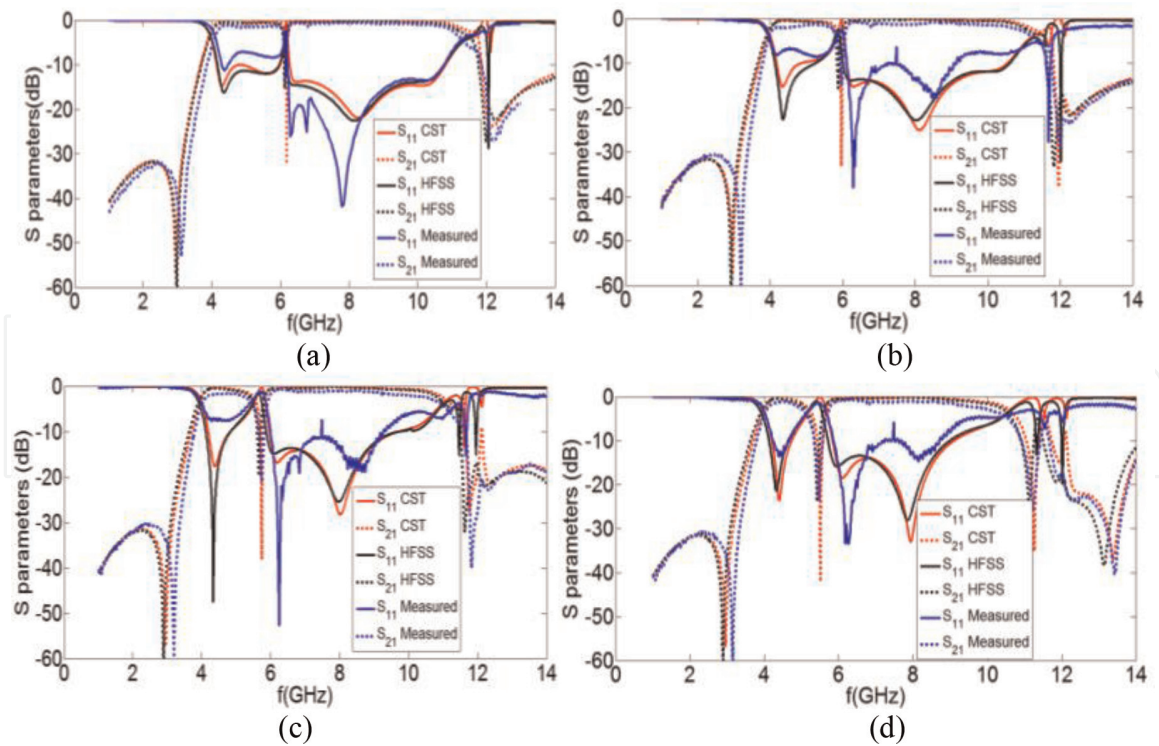

Figure 19.
A photo for the fabricated filter [48].

Figure 20.
The simulated and measured S_{11} and S_{21} for different L_6 lengths, (a) L_6 = 2.0 mm, (b) L_6 = 3.1 mm, (c) L_6 = 4.2 mm, and (d) L_6 = 5.3 mm [48].

different stub lengths (L_6 = 2.2, 3.1, 4.2 and 5.3 mm). The overall dimension of the filter is 16.4 × 5 mm, which is considered very compact compared to other published designs with the same characteristics. **Figure 20(a)** shows the measured and simulated S_{11} and S_{21} with L_6 = 2 mm and f_{notch} = 6.18 GHz. **Figure 20(b)** shows the measured and simulated S_{11} and S_{21} with L_6 = 3.1 mm and f_{notch} = 5.9 GHz. **Figure 20(c)** shows the measured and simulated S_{11} and S_{21} with L_6 = 4.2 mm and f_{notch} = 5.7 GHz. **Figure 20(d)** shows the measured and simulated S_{11} and S_{21} with L_6 = 5.3 mm and f_{notch} = 5.5 GHz. Good agreement was found between the measured data and simulated results.

4.2 Electronically switchable ultra-wide band/dual-band band-pass filter using defected ground structures

Ref. [50] proposed a suitable UWB to dual-band band-pass filter with defected ground structure DGS. This filter consists of four parts, namely, meandered inter digital coupled line sections, stepped impedance open stubs, coupled lines, and rectangular DGS. The filter is miniaturized and has a total area of 12.5 × 10 mm, **Figure 21**. This filter is fabricated on Duroid Teflon substrate with a dielectric constant of 2.2 and a dielectric height of 0.7874 mm. The UWB mode extends from 3.6 up to 10.6 GHz with attenuation greater than 20 dB up to 18 GHz (upper stopband). The dual passbands extended from 3.8 up to 18 GHz (upper stopband). The dual passbands extend from 3.8 up to 5 GHz and from 9.5 up to 10.8 GHz. The proposed filter suppresses WiMAX and X (military) band of satellite that extends from 7 up to 8 GHz. The filter is designed, fabricated, and measured. The mode of the filter is changed by using suitable matrix equipment [50].

DGS at input and output ports of the proposed filter produces two resonances at 7.5 and 9.6 GHz and improve the performance of proposed filter while an overall size reduction of 20% is obtained. The meander lines and stepped impedance open stub are also used to reduce the overall size. By adjusting the connection between
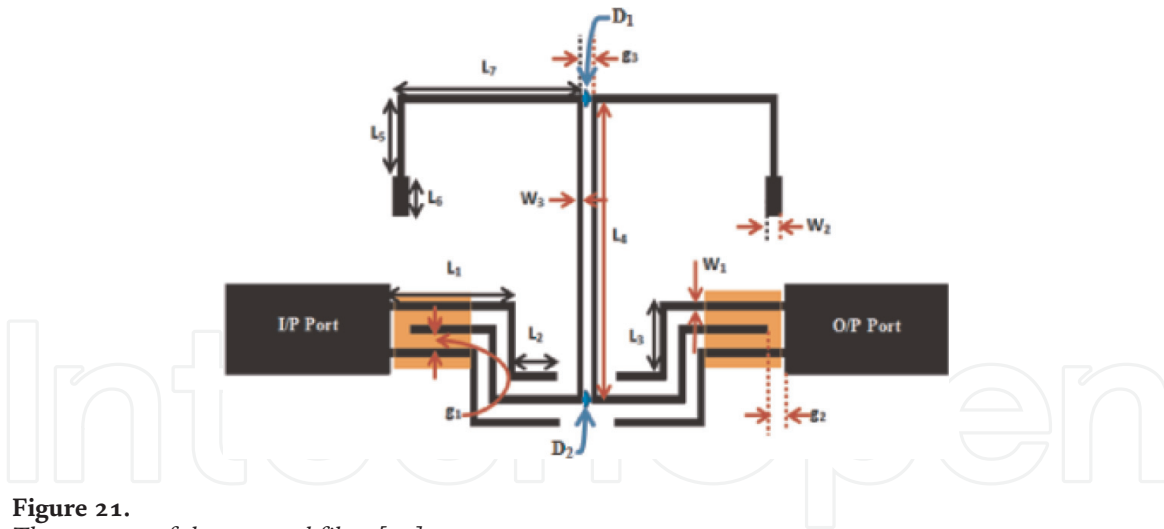
Figure 21.
The structure of the proposed filter [50].

the coupled lines in the center of the design, the center frequency and 3 dB frequency band can be easily adjusted. The proposed filter achieves UWB performance with good selectivity and low insertion loss in the passband from 3.6 to 10.5 GHz and good stopband from 10.6 to 18 GHz. Moreover, it achieves dual bands with good stopband from 5 to 9.5 GHz and from 10.8 to 18 GHz by using open circuit stub to suppress unwanted interference signals in the band of WLAN, WIMAX, and X (Military) band of satellite. All dimensions of the proposed filter are as follows: L_1 = 3.75 mm, L_2 = 1.95 mm, L_3 = 1.8 mm, L_4 = 7.5 mm, L_5 = 2.1 mm, L_6 = 1 mm, L_7 = 5.65 mm, W_1 = 0.2 mm, W_2 = 0.5 mm, W_3 = 0.15 mm, g_1 = 0.2 mm, g_2 = 0.2 mm, and g_3 = 0.3 mm. The simulated S_{11} and S_{21} are shown in **Figure 24**.

4.2.1 The equivalent lumped circuit model analysis of the proposed design

Figure 22 shows the equivalent lumped circuit model of the proposed UWB BPF that is shown in **Figure 21**. The equivalent lumped circuit model results are obtained using circuit model tool of the Advanced Design System (ADS) 2017. The lumped element values are manually optimized by changing each element value, so that it can have good agreement with the simulated results obtained from the full wave simulator.

The whole equivalent circuit of the proposed filter can be divided into the following subsections: DGS part at input and output ports, interdigital coupled lines and stepped impedance open stub. As shown in the lumped element model (**Figure 22**), R_{d1}, C_{d1}, L_{d1}, R_{d2}, C_{d2}, and L_{d2} represent the equivalent resistance,
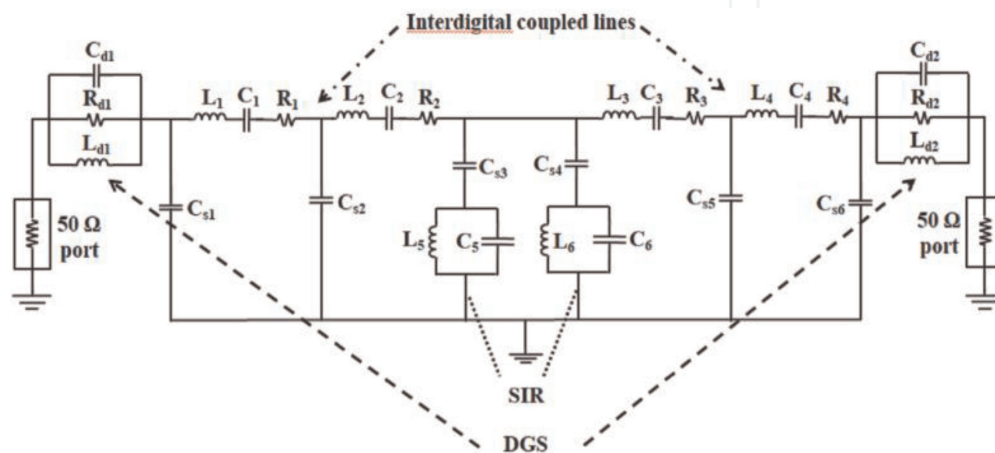

Figure 22.
*Equivalent lumped circuit model of the proposed UWB BPF shown in **Figure 21** [50].*

inductance, and capacitance of the defected ground structure (DGS) [51]. L_5, C_5, L_6, and C_6 represent the equivalent inductance and capacitance of the stepped imped-ance resonator (SIR). Interdigital coupled arm is represented by the series capaci-tance with parasitic inductance and resistance, and shunt capacitances [52] as shown in **Figure 22**. The S-parameters versus frequency response of EM simulation and circuit model are compared. There is a very good agreement between the simulated and equivalent lumped circuit model results.

4.2.2 Fabrication and measurements

Photolithographic technique was used to fabricate this filter on Teflon substrate (Duroid RT 5880) with physical properties of ε_r =2.2 and tan∂ = 0.0009, while the dielectric thickness is 0.7874 mm. **Figure 23** shows a photograph for the fabricated filter for both sides (the front and back sides). The soldered wires shown in **Figure 23** are used to connect the filter with diode switch matrix tool. The filters are measured using the vector network analyzer (N9928A FieldFox Handheld Micro-wave Vector Network Analyzer, 26.5 GHz) [50].

Figure 24(a) shows the measured and simulated results of the proposed filter at ON state with frequency range from 1 to 20 GHz. It should be noted that the frequency range is extended up to 20 GHz in order to show that the out of band rejection is good, and the measured 3 dB passband of the proposed filter is between 3.6 and 10.6 GHz. **Figure 24(b)** shows the measured and simulated results of the proposed filter at OFF state, and the dual bands with 3 dB passbands extend from 3.8 to 5 GHz and from 9 to 10.8 GHz [50].
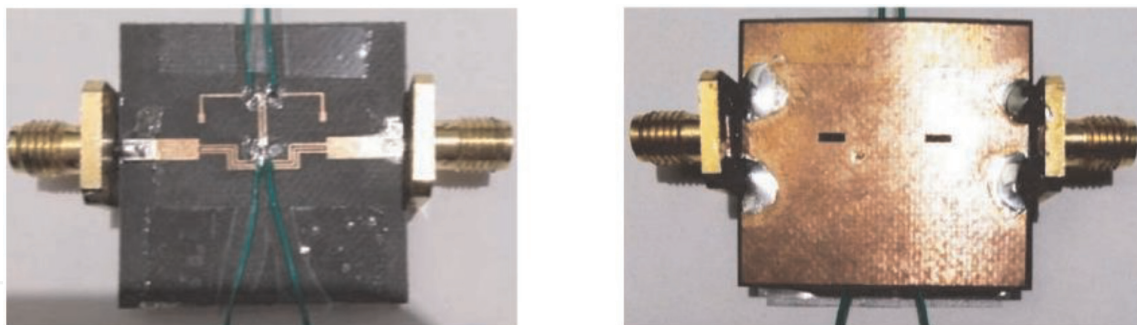

Figure 23.
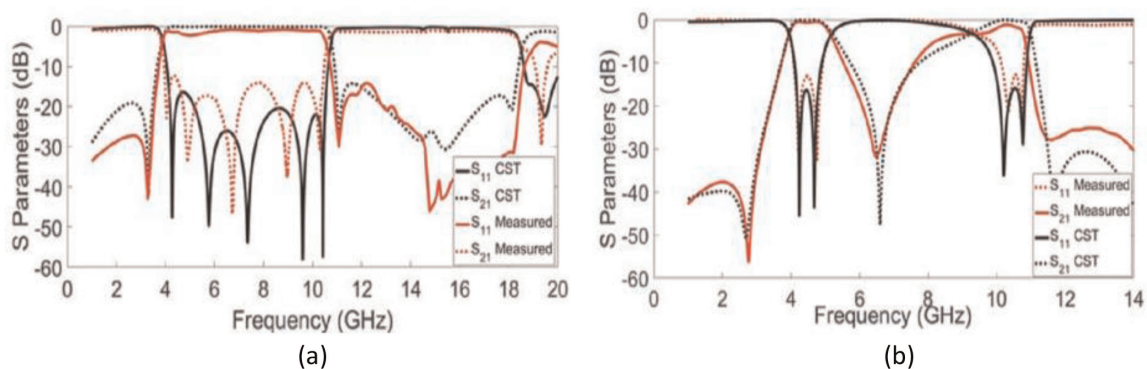*A photo for the fabricated filter [50].*

Figure 24.
The simulated and measured S_{11} and S_{21} without O.C stub. (a) D1 and D2 ON state (with frequency range from 1 to 20 GHz) and (b) D1 and D2 OFF state [50].
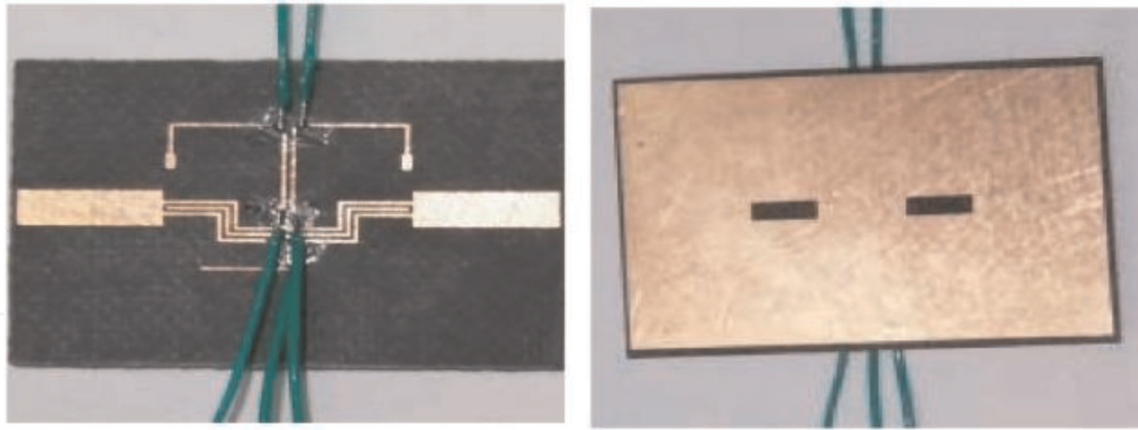
Figure 25.
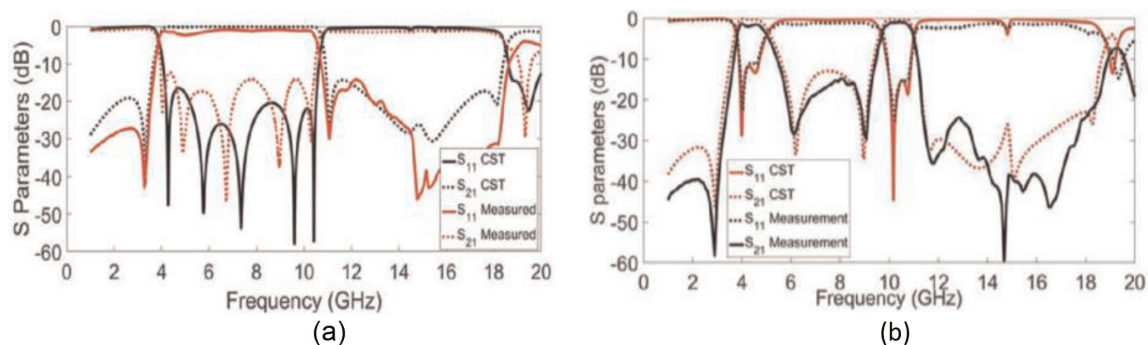*A photo for the fabricated filter of **Figure 10**.*

Figure 26.
The simulated and measured S_{11} and S_{21} with O.C stub. (a) D1, D2 ON, and D3 OFF, (b) D1, D2 OFF and D3 ON [50].

Photos for the fabricated filter with open stub are shown in **Figure 25**. **Figure 26 (a)** shows the measured and simulated results of the proposed filter with open stub at D1, D2 ON state, and D3 OFF with frequency range from 1 to 20 GHz. It should be noted that the out of band rejection is good, and the measured 3 dB passband of the proposed filter is between 3.6 and 10.6 GHz. **Figure 24(b)** shows the measured and simulated results of the proposed filter with open stub at D1, D2 OFF state and D3 ON, and the dual bands with 3 dB passbands extend from 3.8 to 5 GHz and from 9.5 to 10.8 GHz [50].

5. UWB filtenna

In general, the filtenna consists of a filter and antenna that are combined in one structure. The proposed filtenna operates at three bands of frequency (2.4, 5.5, and 28 GHz) to cover the 4G/5G communication system. It consists of three parts, namely, Franklin strip monopole antenna to cover 4G, WLAN, and WiMAX and a rectangular patch antenna to cover 5G band. The third part consists of a modified CMRC low-pass filter that exists between the two antenna parts to isolate the Franklin antenna from the rectangular patch antenna at 5G band. It also allows feeding the Franklin antenna at low frequency bands. The total size of the filtenna is $45 \times 40 \times 0.508$ mm^3 and fabricated on Teflon dielectric substrate (Roger 5880). The proposed filtenna has wide impedance bandwidth (15.8, 23.5, and 11.3%) and high gain (1.95, 3.76, 7.35 dBi) [53]. The proposed multiband filtenna is shown in **Figure 27**.
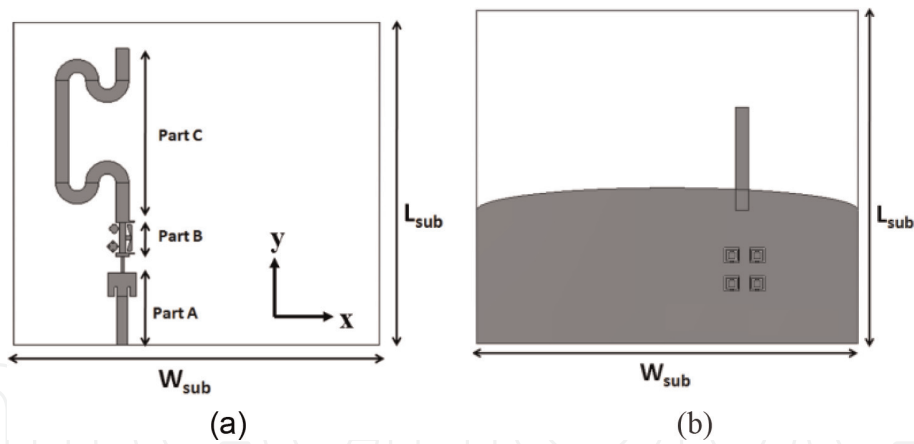
Figure 27.
The proposed multiband filtenna (a) front view and (b) back view [53].

5.1 Modified CMRC LPF using novel fractal patches

A modified compact microstrip resonance cell (CMRC) low-pass filter (LPF) using novel fractal patches was proposed in [54], see **Figure 28**. The fractal patches produce additional transmission zeros to the stop-band, while the open-ended stubs cause an extension in the stopband achieving a compact ultrawide and deep stopband filter with good selectivity and low insertion loss in the passband. The results show −10 dB bandwidth from 3.3 to 67 GHz with 181.5% relative stopband bandwidth. The 3-dB cutoff frequency is 2.85 GHz and less than 1.5 dB insertion loss in the passband and 0.55 GHz transaction from −3 to −20 dB and − 20 dB suppression from 3.5 to 67 GHz, so that the filter can be expected to suppress the unwanted harmonics and prevent inter-modulation with the new systems with high frequency operating bands. The filter has been designed on a Rogers 5880 substrate with a relative dielectric constant of 2.2, substrate thickness of 0.508 mm, and 0.0009 loss tangent. **Figure 28** shows the proposed filter design, and it consists of two traditional triangle taper resonance cells in one side of the transverse connecting narrow width transmission line which has almost the same performance of the complete CMRC structure, while two different sizes circular fractal patches are present on the other half. Each fractal consists of main circular patch and additional small circular patches at edges. The two fractals act as a dual behavior resonator to have additional transmission zeros in the stopband. Each fractal is resonating at certain frequency in addition with enhancing the low suppression bands of the entire stop-band. Also, four open ended stubs are used to extend the
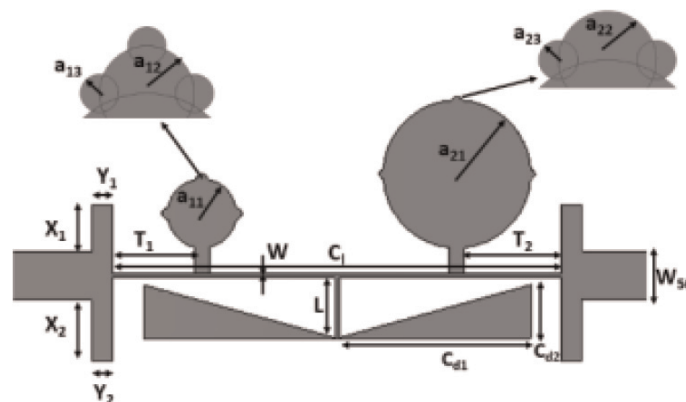

Figure 28.
The design of proposed low-pass filter [53].

stopband by adding new transmission zeros without increasing the circuit size. The main dimensions are given in **Table 6**, all dimensions in millimeter.

5.2 Franklin monopole antenna

Part C of the multiband rectenna system is a Franklin strip monopole dual-band antenna to be used to cover Bluetooth at 2.4 GHz, 4G, LTE bands at 2.3, 2.5 and 2.6 GHz, WiMAX at 2.5 and 5.5GHz, WLAN at 2.4, 5.2 GHz [53]. The geometry of the antenna is shown in **Figure 29**. The antenna has a rectangular stub on a curved partial ground. The length of the bending strip is about one-half of the guide wavelength at its first resonance frequency. The meander radius and the length of the Franklin strip are mainly determining the two resonance frequencies of the antenna, while the rectangular stub with a length of a quarter wavelength and curved ground have been used to increase the bandwidth of the upper band (5.5 GHz). The L-C equivalent circuit of the Franklin monopole antenna is shown in **Figure 30**. The dimensions of the antenna are shown in **Table 7**, while the equivalent circuit parameters are shown in **Table 8**.

5.3 Rectangular patch antenna

The first part of the rectenna (part A) consists of a rectangular patch antenna with inset feed for matching and four CSRRs (complementary split ring resonator) in the other side (ground plane). This antenna covers the 5G range of frequency (28 GHz). This shape is chosen due to its simplicity and can be placed in the Franklin feeding line. **Figure 31** shows the geometry of the rectangular patch with inset feeding. The final dimensions of the antenna after using optimization techniques of the CST simulator are introduced in **Table 9**. The L-C equivalent circuit of this antenna with CSRRs is shown in **Figure 32**. The rectangular patch is

Parameter	C_l	L	W	C_{d1}	C_{d2}	a_{11}	a_{12}	a_{13}	a_{21}
Value (mm)	17.6	2.4	0.15	7.6	2.1	1.35	0.2	0.05	2.9
Parameter	a_{22}	a_{23}	X_1	X_2	Y_1	Y_2	T_1	T_2	W_{50}
Value (mm)	0.15	0.05	2.4	1.8	0.8	0.8	3.2	3.8	1.6

Table 6.
Circuit dimensional parameters [53].

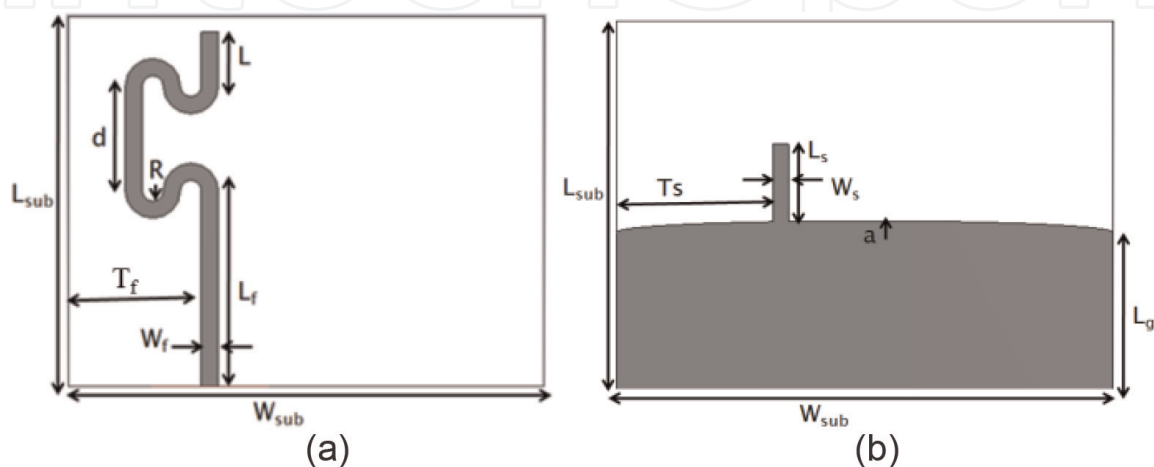(a)   (b)

Figure 29.
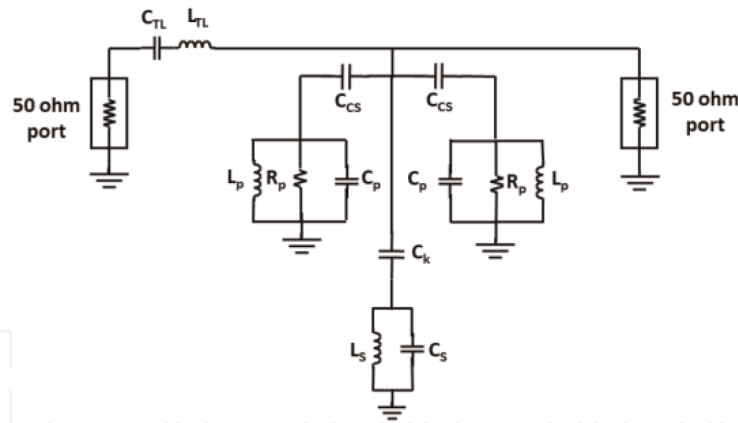*The design of the proposed Franklin strip monopole antenna (a) front and (b) back [53].*

Figure 30.
The equivalent LC circuit of the proposed 4G Franklin monopole antenna,

L_{sub}	W_{sub}	L_f	L_g	L	d
35	45	18.5	14.9	5.1	9.9
R	a	W_f	W_s	T_f	T_s
1	1.1	1.6	1.5	13.4	14.9

Table 7.
Dimensions of the proposed Franklin antenna (all dimensions in mm) [53].

CTL	LTL	Cp	Lp	Rp	CS	LS	Ck	Ccs
2	1.7	2606	0.0007	0.05	0.1	0.05	18.4	42.4
C in Pico Farad, L in Nano Henry and R in ohm.								

Table 8.
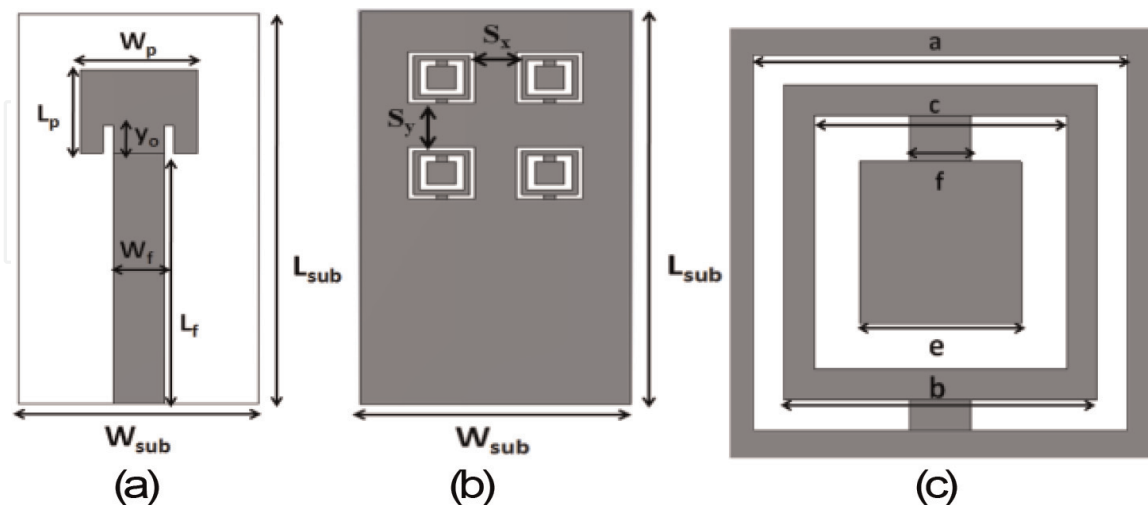*Franklin monopole antenna equivalent circuit parameters [53].*

Figure 31.
The design of 5G rectangular patch antenna. (a) Front view, (b) back view, and (c) the dimensions of the CSRR [53].

represented as two radiating slots each one represented by a parallel R L C circuit, while each one of the four CSRRs represented by parallel LC and the electric coupling between the CSRRs on the ground and radiating patch on the top side is represented by capacitor C_k and the magnetic coupling represented by the mutual

L$_{sub}$	W$_{sub}$	L$_f$	W$_f$	y$_o$	L$_p$	W$_p$
11	7.5	6	1.6	1	2.95	3.45
S$_x$	S$_y$	a	b	c	e	f
1.15	1.55	1.85	1.55	1.25	0.8	0.3

Table 9.
5G antenna dimensional parameters (all dimensions in mm).
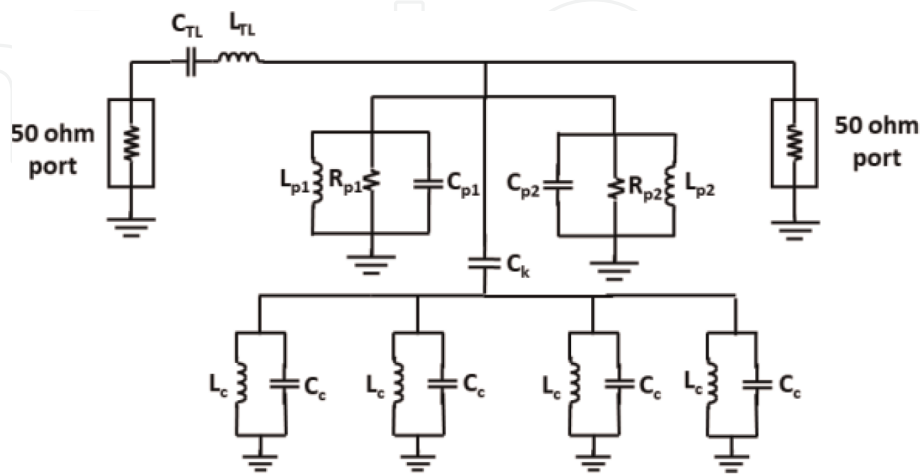
Figure 32.
(a) The equivalent LC circuit of the proposed 5G rectangular patch antenna [53].

C$_{TL}$	L$_{TL}$	C$_{p1}$	L$_{p1}$	R$_{p1}$	C$_{p2}$	L$_{p2}$	R$_{p2}$	C$_c$	L$_c$
17.5	0.16	1.06	0.26	93.6	10^{-12}	0.02	54.9	0.79	1.2

C *in Pico farad, L in Nano Henry and R in ohms.*

Table 10.
5G antenna equivalent circuit parameters.

inductance offered by the ADS software. All lumped element values are listed in **Table 10** [53].

5.4 Simulation and measurement results of filtenna

The equivalent circuit model simulation results of the filtenna system shown in **Figure 27** is determined by merging the three parts component's equivalent circuit,
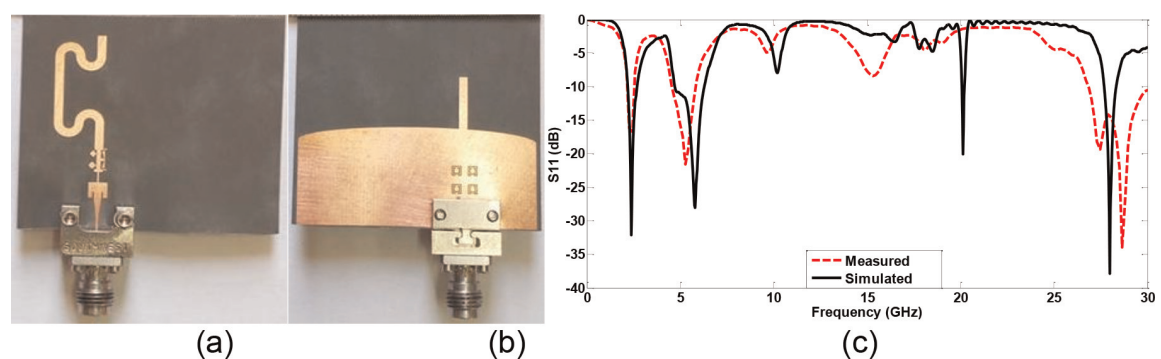

Figure 33.
Photograph of fabricated antenna. (a) Front view, and (b) back view and (c) the measured and simulated reflection coefficient [53].
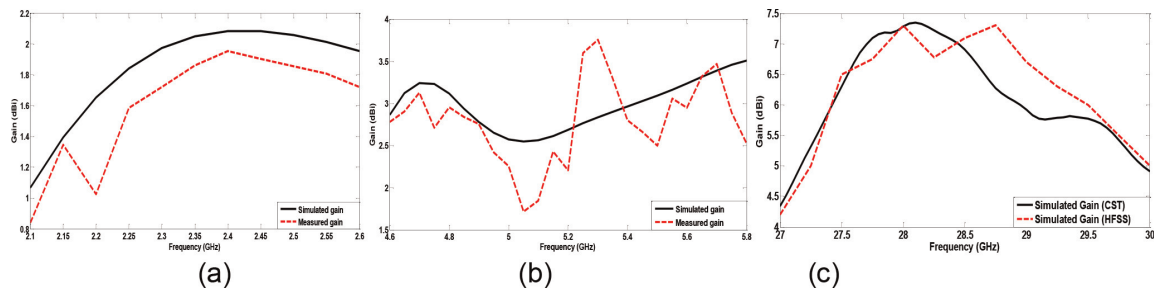
Figure 34.
Simulated and measured gain at: (a) first band, (b) second band, and (c) simulated gain using CST and HFSS simulators for the third band [53].

namely, 5G rectangular patch antenna, modified CMRC low-pass filter, and 4G Franklin monopole antenna extract using ADS software [53]. The filtenna was fabricated using the photolithographic technique.

Figure 32 shows a photo of the fabricated rectenna. The simulated and measured reflection coefficient is shown in **Figure 33**. The measured results show that the filtenna has −10 dB impedance of the first band from 2.16 to 2.53GHz, the second band is from 4.58 to 5.8GHz, and the third band is from 26.8 GHz to 30 GHz. The simulated and measured gains are shown in **Figure 34**. The first and second bands have peak measured gain level of 1.95 and 3.76 dBi, respectively. The third band achieves 7.35 dBi peak simulated gain level [53].

Author details

Dalia N. Elsheakh* and Esmat A. Abdallah
Microstrip Department, Electronics Research Institute, Giza, Egypt

*Address all correspondence to: daliaelsheakh@gmail.com

IntechOpen

References

[1] Federal Communication Commission. First Report and Order-Revision of Part 15 of the Commission's Rules Regarding Ultra-Wideband Transmission System. FCC 02 48; 2002

[2] Zhang Q. Ultra-Wideband Impulse Radio Communication System Design and Prototyping. USA: Tennessee Technological University;

[3] Qiu RC, Liu HP, Shen X. Ultra-wideband for multiple access. IEEE Communications Magazine. 2005;**43**: 80-87

[4] Qiu RC. A study of the ultra-wideband wireless propagation channel and optimum UWB receiver design, Part I. IEEE Journal on Selected Areas in Communications. 2002;**20**(9):1628-1637

[5] Chong C-C, Watanabe F, Inamura H. Potential of UWB technology for the next generation wireless communications. In: IEEE Ninth Inter-National Symposium on Spread Spectrum Techniques and Applications; Manaus, Amazon, Brazil. 2006

[6] Fakharzadeh M, Mohajer M. An integrated wide-band circularly polarized antenna for millimeter-wave applications. IEEE Transactions on Antennas and Propagation. 2014;**62**: 925-929

[7] Pinel S, Kim K, Yang K, Laskar J. 60 GHz linearly and circularly polarized antenna arrays on liquid crystal polymer substrate. In: Proceedings of 36th European Microwave Conference. 2006. pp. 858-861

[8] Yeung SH, Man KF, Chan WS. A bandwidth improved circular polarized slot antenna using a slot composed of multiple circular sectors. IEEE Transactions on Antennas and Propagation. 2011;**59**: 3065-3070

[9] James JR, Hall PS, editors. Handbook of Microstrip Antennas. London: Peter Peregrinus; 1989

[10] Hall PS, Dahele JS. Dual and circularly polarized microstrip antennas. In: Lee KF, Chen W, editors. Advances in Microstrip and Printed Antennas. New York: Wiley; 1997

[11] Hsu CL, Hsu FC, Kuo JT. Microstrip bandpass filters for ultra-wideband (UWB) wireless communications. In: IEEE MTT-S International Microwave Symposium Digest. 2005. pp. 679-682

[12] Hong JS, Shaman H. An optimum ultra-wide-band microstrip filter. Microwave and Optical Technology Letters. 2005;**47**:230-233

[13] Li X, Ji X. Novel compact UWB bandpass filters design with cross-coupling between short-circuited stubs. IEEE Microwave and Wireless Components Letters. 2014;**24**(1):23-25

[14] Zhu L, Sun S, Menzel W. Ultra-wideband (UWB) bandpass filters using multiple-mode resonator. IEEE Microwave and Wireless Components Letters. 2005;**15**(11):796-798

[15] Xu J, Wu W, Kang W, Miao C. Compact UWB bandpass filter with a notched band using radial stub loaded resonator. IEEE Microwave and Wireless Components Letters. 2012;**22**(7):351-353

[16] Shaman H, Hong JS. Ultra-wideband (UWB) bandpass filter with embedded band notch structure. IEEE Microwave and Wireless Components Letters. 2007;**17**(3):193-195

[17] Kim CH, Chang K. Ultra-wideband (UWB) ring resonator bandpass filter with a notched band. IEEE Microwave and Wireless Components Letters. 2011; **21**(4):206-208

[18] Wong SW, Zhu L. Implementation of compact UWB bandpass filter with a notch-band. IEEE Microwave and Wireless Components Letters. 2008;**18**(1):10-12

[19] Yang G-M, Jin R, Vittoria C, Harris VG, Sun NX. Small ultra-wideband (UWB) bandpass filter with notched band. IEEE Microwave and Wireless Components Letters. 2008;**18**(3):176-178

[20] Hao Z-C, Hong J-S, Parry JP, Hand DP. Ultra-wideband bandpass filter with multiple notch bands using nonuniform periodical slotted ground structure. IEEE Transactions on Microwave Theory and Techniques. 2009;**57**(12):3080-3088

[21] García RG, Guyette AC. Reconfigurable multi-band microwave filters. IEEE Transactions on Microwave Theory and Techniques. 2015;**63**(4): 1294-1307

[22] Wang H, Tam KW, Ho SK, Kang W, Wu W. Design of ultra-wideband bandpass filters with fixed and reconfigurable notch bands using terminated cross-shaped resonators. IEEE Transactions on Microwave Theory and Techniques. 2014;**62**(2):252-265

[23] Horestani AK, Shaterian Z, Naqui J, Martín F, Fumeaux C. Reconfigurable and tunable S-shaped split-ring resonators and application in band-notched UWB antennas. IEEE Transactions on Antennas and Propagation. 2016;**64**(9):3766-3776

[24] Liang JG, Zhang X, Sun L. Compact UWB bandpass filter with triple notched bands using quadruple-mode resonator. In: IEEE International Conference on Microwave and Millimeter Wave Technology (ICMMT). Vol. 1. Beijing, China; 2016. pp. 354-356

[25] Zheng X, Liu W, Zhang X, Jiang T. Design of dual band-notch UWB

bandpass filter based on T-shaped resonator. In: Progress in Electromagnetic Research Symposium; 8-11 August 2016; Shanghai, China. 2016. pp. 4482-4486

[26] Ahmed KU, Virdee BS. Ultra-wide band bandpass filter based on composite right/left handed transmission-line unit cell. IEEE Transactions on Microwave Theory and Techniques. February 2013; **61**(2):782-788

[27] Elsheakh DN. Linear/circular polarization slot antennas for millimeter wave application. Microwave and Optical Technology Letters. 2017;**59**(4): 976-983

[28] Madhuri S, Tiwari VN. Review of circular polarization techniques for design of microstrip patch antenna. Conference: International Conference on Recent Cognizance in Wireless Communication & Image Processing, Jaipur, 2014

[29] Pozar DM, Schaubert DH. Microstrip Antennas: The Analysis and Design of Microstrip Antennas and Arrays. New York: IEEE Press; 1995

[30] Nesic D, Nesic A, Brankovic V. Circular polarized printed antenna with broadband axial ratio. In: Presented at the IEEE Antennas Propagation Society International Symposium. 2003. pp. 912-915

[31] Li RL, Dejean G, Laskar J, Tentzeris MM. Investigation of circularly polarized loop antennas with a parasitic element for bandwidth enhancement. IEEE Transactions on Antennas and Propagation. 2005;**53**: 3930-3939

[32] Weily AR, Guo YJ. Circularly polarized ellipse-loaded circular slot array for millimeter-wave WPAN applications. IEEE Transactions on Antennas and Propagation. 2009;**57**: 2862-2870

[33] Wong K-L. Compact and Broadband Microstrip Antennas. 1st ed. New York: Wiley-Interscience; 2002

[34] Sun H, Guo YX, Wang Z. 60-GHz circularly polarized U-slot patch antenna array on LTCC. IEEE Transactions on Antennas and Propagation. 2013;**61**:430-435

[35] Nakano H, Eto J, Okabe Y, Yamauchi J. Tilted and axial beam formation by a single-arm rectangular spiral antenna with compact dielectric substrate and conducting plane. IEEE Transactions on Antennas and Propagation. 2002;**50**:17-23

[36] Bayat A, Mirzakhani R. A parametric study and design of the balanced antipodal Vivaldi antenna (BAVA). In: PIERS Proceedings; 19-23 August 2012; Moscow, Russia. 2012. pp. 778-782

[37] Agahi MH, Abiri HL, Mohajeri F. Investigation of a new idea for antipodal Vivaldi antenna design. International Journal of Computer and Electrical Engineering. 2011;**3**(2):1793-8163

[38] Zhang F, Fang G-Y, Ji YC, Ju H-J, Shao J-J. A novel compact double exponentially tapered slot antenna (DETSA) for GPR applications. IEEE Antennas and Wireless Propagation Letters. 2011;**10**:195-198

[39] Elsheakh DN, Abdallah EA. Compact printed log-periodic dipole antenna for terrestrial digital video broadcast (DVB-T) application. Microwave and Optical Technology Letters. 2014;**56**:1002-1007

[40] Lin S, Luan S, Wang YD, Luo X, Han X, Zhang XQ, et al. A printed log periodic tree dipole antenna (PLPTDA). Progress in Electromagnetics Research M. 2011;**21**:19-32

[41] Wu J, Zhao Z, Nie Z, Liu QH. A printed UWB vivaldi antenna using

stepped connection structure between slot line and tapered patches. IEEE Antennas and Wireless Propagation Letters. 2014;**13**:698-701

[42] Yu C, Hong W, Chiu L, Zhai G, Yu C, Qin W, et al. Ultrawideband printed log-periodic dipole antenna with multiple notched bands. IEEE Transactions on Antennas and Propagation;**59**:725-732

[43] Casula G, Maxia P, Mazzarella G, Montisci G. Design of a printed log periodic dipole array for ultra-wideband applications. Progress in Electromagnetics Research C. 2013;**38**:15-26

[44] Pozar DM, Kaufman B. Comparison of three methods for the measurement of printed antenna efficiency. IEEE Transactions on Antennas and Propagation. 1988;**36**:136-139

[45] Elsheakh DM, Abdallah EA. Ultra-wide-bandwidth (UWB) microstrip monopole antenna using split ring resonator (SRR) structure. International Journal of Microwave and Wireless Technologies. 2018;**1**:1-10

[46] Erentok A, Ziolkowski RW. Metamaterial-inspired efficient electrically small antennas. IEEE Transactions on Antennas and Propagation. 2008;**56**:691-707

[47] Erentok A, Ziolkowski RW. Two-dimensional efficient metamaterial-inspired electrically small antenna. Microwave and Optical Technology Letters. 2007;**49**:1669-1673

[48] Ouf EG, Mohra AS, Abdallah EA, Elhennawy H. Ultra-wideband bandpass filter with sharp tuned notched band rejection based on CRLH transmission-line unit cell. Progress in Electromagnetics Research Letters. 2017;**69**:9-14

[49] Ahmed KU, Virdee BS. Ultrawide band bandpass filter based on composite

right/left handed transmission line unit cell. IEEE Transactions on Microwave Theory and Techniques. 2013;**61**(2): 782-788

[50] Ouf EG, Mohra AS, Abdallah EA, Elhennawy H. Electronically switachable ultra-wide band/dual-band bandpass filter using defected ground structures. Progress in Electromagnetics Research C. 2019;**91**:83-96

[51] Sarkar D, Moyra T, Murmu L. An ultra-wideband (UWB) bandpass filter with complementary split ring resonator for coupling improvement. International Journal of Electronics and Communications. 2017;**71**:89-95

[52] Weng LH, Guo Y-C, Shi X-W, Chen X-Q. An overview on defected ground structure. Progress in Electromagnetics Research B. 2008;**7**: 173-189

[53] Yassin ME, Mohamed HA, Abdallah EA, Elhennawy H. Single fed 4G/5G multiband 2.4/5.5/28GHz antenna. IET Microwaves, Antennas and Propagation. March 2018;**13**: 286-290

[54] Yassin ME, Mohamed HA, Abdallah EA, Elhennawy H. Modified CMRC LPF using novel fractal patches. Progress in Electromagnetics Research Letters. 2018;**79**:25-31